Environmental Earth Sciences (2021) 80:448
https://doi.org/10.1007/s12665-021-09738-9

ORIGINAL ARTICLE

Machine learning models to estimate the elastic modulus of weathered magmatic rocks

Nurcihan Ceryan[1] · Erkan Caner Ozkat[2] · Nuray Korkmaz Can[3] · Sener Ceryan[4]

Received: 18 October 2020 / Accepted: 7 June 2021 / Published online: 17 June 2021

Abstract

In recent years, several soft computing models have been proposed to estimate the elastic modulus of magmatic rocks. However, there are lacks in models that consider the different weathering degrees in determining the elastic modulus of rocks. In the literature, mechanical properties are widely used as inputs in predictive models for weathered rocks; however, there are only a few models that use index properties representing the effect of weathering on magmatic rocks. In this study, support vector regression (SVR) Gaussian process regression (GPR), and artificial neural network (ANN) models were developed to predict the elastic modulus of magmatic rocks with different degrees of weathering. The inputs selected by the best subset regression approach were porosity, P-wave velocity, and slake durability index. Key performance indicators (KPIs) were computed to validate the accuracy of the developed models. In addition to KPIs, Taylor diagrams and regression error characteristic (REC) curves were used to assess the performance of the developed prediction models. In this study, considering the difficulties of expressing the error using only RMSE and MAE, a new performance index (PI), PI_{MAE}, was proposed using normalized MAE instead of normalized RMSE. It was also indicated that PI_{RMSE} and PI_{MAE} should be used together in performance analysis. When considering the Taylor diagram, PI_{RMSE}, and PI_{MAE}, the GPR models performed best, and the SVR model performed the worst in both the training and test periods. Similarly, according to the REC curve in both periods, the performance of the SVR was the worst, while the performance of the ANN model was the best. The PI_{RMSE} and PI_{MAE} values of the GPR model for the test data were 1.3779 and 1.4142, respectively, and they were 1.2567 and 1.4139, respectively, for the ANN model. According to the computed response surfaces, an increase in the P-wave velocity, and a decrease in the porosity increased the elastic modulus. However, changes in slake durability index only had a minor effect on the elastic modulus.

Keywords Elastic modulus · Weathered magmatic rocks · Machine learning · Porosity · *P*-wave velocity · Slake durability index

Introduction

Natural rock masses consist of intact rock blocks separated by discontinuities. Therefore, the mechanical properties of intact rock, the geotechnical properties of discontinuities, and the rock mass structure are the most important parameters affecting the engineering deformation properties of rock masses. It is also known that weathering significantly affects these engineering properties of rocks (Ceryan 2015). One of the most important intact rock properties affecting the engineering behavior of rock mass is the elastic modulus (E_s) just as uniaxial compressive strength (UCS), and Poisson ratio (ν). Therefore, E_s of intact rock is generally used as an input in both numerical models and in empirical relationships to evaluate the engineering behavior of rock

✉ Erkan Caner Ozkat
erkancaner.ozkat@erdogan.edu.tr

[1] Department of Mining and Mineral Extraction, Balikesir Vocational School, Balikesir University, Balikesir, Turkey

[2] Faculty of Engineering and Architecture, Department of Mechanical Engineering, Recep Tayyip Erdogan University, Rize, Turkey

[3] Department of Mechanical Engineering, Istanbul University-Cerrahpasa, Istanbul, Turkey

[4] Department of Geological Engineering, Balıkesir University, Balikesir, Turkey

masses (Kayabasi et al. 2003; Sonmez et al. 2006; Hoek and Diederichs 2006; Bidgoli et al. 2013; Zhang 2017; Saedi et al. 2019; Alemdag et al. 2016).

UCS tests, standardized by the International Society for Rock Mechanics (ISRM), are utilized to measure the E_s and UCS of rock materials directly. The tests require well-prepared rock specimens that cannot always be extracted from weak, thinly bedded, stratified, highly fractured, highly weathered, high-porosity, clay-containing, coarse-grained, and block-in-matrix rocks. Furthermore, the tests are expensive, complicated, time-consuming, and require sophisticated and expensive instruments (Gokceoglu and Zorlu 2004; Xia et al. 2014; Ko et al. 2016), making it difficult to evaluate E_s using standard laboratory tests. To overcome these difficulties for directly measuring E_s, regression models have been developed (Nefeslioglu 2013; Ozkat et al. 2017a,b; Aboutaleb et al. 2018; Mashayekhi et al. 2020). The independent variables (i.e., the inputs) used in these models, are commonly the physical properties of rock samples that can be measured easily and cheaply. These simple and non-destructive index properties include the elastic wave velocity (Kurtuluş et al. 2010; Brotons et al. 2016), porosity, effective porosity, void ratio, unit weight, density, and water saturation (Tugrul 2004; Yilmaz and Yuksek 2008; Erguler and Ulusay 2009; Marques et al. 2010; Wang et al. 2014; Kim et al. 2017). Other inputs derived from the index tests are the slake durability index (Yagiz et al. 2012; Ceryan 2014; Ghasemi et al. 2018), weathering indices (Ceryan 2015, 2016), texture coefficient, and mineral content; especially determining quartz, plagioclase, and clay content (Shakoor and Bonelli 1991; Singh and Verma 2012; Pan et al. 2013; Diamantis et al. 2014; Heap et al. 2014; Undul and Florian 2015; Ajalloeian et al. 2017). Simple mechanical test results, including the Schmidt hammer rebound hardness, the point loading index, tensile strength, the blocked punch index, and the cylindrical punch index are also employed in regression models (Dinçer et al. 2004; Karakus et al. 2005; Yilmaz and Yuksek 2009; Khandelwal and Singh 2011; Singh and Verma 2012; Singh et al. 2012; Alikarami et al. 2013; Armaghani et al. 2015; Saedi et al. 2018; Mahdiabadi and Khanlari 2019).

Conventional regression methods, such as simple linear regression and multi-linear regression methods, are widely used in the literature to estimate E_s. In general, the equations obtained with conventional regression methods are recommended only for specific rock types (Fener et al. 2005; Beiki et al. 2013). If new data are substantially different from the original data, the form of the obtained equations needs to be updated. Moreover, in some cases, the prediction results are inadequate (Sonmez et al. 2006; Yilmaz and Yuksek 2009; Beiki et al. 2013; Rezaei et al. 2014). Considering these difficulties in the prediction of E_s using conventional regression methods, many researchers have employed soft computing methods (Table 1).

The main purpose of this study is to examine the applicability and capability of Support Vector Regression (SVR), Gaussian Process Regression (GPR), and Artificial Neural Network (ANN) models in the E_s prediction of magmatic rocks with different degrees of weathering. The inputs, porosity (n), P-wave velocity (V_p), and slake durability index (I_d) used in the proposed models were determined by the best subset regression method, and the performances of these models were evaluated with the maximum determination coefficient (R^2), Root Mean Square Error (RMSE), normalized RMSE (NRMSE), Mean Absolute Error (MAE), normalized MAE (NMAE), Mean Squared Error (MSE), Nash–Sutcliffe coefficient (NS), Variance Account Factor (VAF), Performance Index (PI), Regression Error Characteristic Curve (REC), and Taylor diagrams.

The remainder of the paper is organized as follows: "Materials and experimental details" describes the materials and experimental procedures; "Problem formulation" defines the inputs and output and explains the proposed regression models. The results and discussions are introduced in "Results" and "Discussion", respectively. The conclusions are presented in "Conclusion".

Materials and experimental details

The sample blocks in the present study were gathered from three different formation/lithodemes exposed in the Eastern Pontides, NE Turkey. They mainly consisted of (1) Late Cretaceous volcanic rocks, (2) volcano-sedimentary rock aged Eosen, and (3) granitic rocks (Fig. 1).

The tests for Schmidt hardness, specific gravity, slake durability, P-wave velocity, and UCS were conducted according to standards defined by ISRM (2007). The core samples used in these tests were extracted from block samples that had different degrees of weathering (Fig. 2). The index properties and modulus of elasticity of the samples used in this study are presented in Table 2.

The N-type rebound hammer was used in the Schmidt hammer test to determine the hardness value (SHH). The SHH $\times \gamma$ term (Deere and Miller 1966; Aufmuth 1974) was obtained by multiplying the measured hardness values (SHH) by unit weight (γ). The grain density $\left(\rho_s\right)$ was determined by employing the specific gravity test, and the dry density was obtained experimentally. Subsequently, the porosity value (n) was calculated using Eq. (1).

$$n = 1 - \frac{\rho_d}{\rho_s} \tag{1}$$

Table 1 Soft computing models proposed to estimate the modulus of elasticity of rock materials

References	Technique	Input	R^2	Rock type
Gokceoglu and Zorlu (2004)	FIS	V_p, BPI, PLI, TS	0.79	Greywacke
Sonmez et al. (2004)	FIS	$VBPr_i$	0.88	Agglomerate
Sonmez et al. (2006)	ANN	UCS, UW	0.67	Different type of rocks
Yilmaz and Yuksek (2008)	ANN	n_e, I_d, SHH, PLI	0.91	Gypsum
Tiryaki (2008)	ANN	ρ, SH, CI	0.50	Magmatic and sedimentary rocks
Yilmaz and Yuksek (2009)	ANN, ANFIS	V_p, PLI, SHH, WC	0.955	Gypsum
Kahraman et al. (2009)	ANN	VBP, ρ, V_p, V_s	0.79	Fault breccia
Heidari et al. (2010)	ANN	UCS, n, ρ, V_p	0.87	Limestone, marl, and dolomite)
Dehghan et al. (2010)	ANN	n, SHH, PLI, V_p	0.77	Travertine
Khandelwal and Singh (2011)	ANN	UCS, TS	0.992	Schistose rocks
Ocak and Seker (2012)	ANN	UCS, UW	–	Different type of rocks
Singh et al. (2012)	ANFIS	ρ, PLI, WA	0.66	Different type of rocks
Yagiz et al. (2012)	ANN	UW, V_p, I_d, SHH, n,	0.81	Carbonate rocks
Manouchehrian et al. (2013)	GP	Q, ρ, n, SH, CI	0.68	Granitic rocks
Kumar et al. (2013)	GPR, RVM, MPMR	SHH, n, V_p, PLI	0.984 0.992 0.914	Travertine
Beiki et al. (2013)	GP	ρ, n, V_p	0.67	Carbonate rocks
Liu et al. (2013)	ANN PSO-SVM	Mnrlgy, PrS, VO, BD, MPf	0.764 0.990	Sandstone
Liu et al. (2014)	ANN SVM RVM	Mnrlgy, PrS, VO, BD, MPf	0.94 0.84 0.98	Sandstone
Ranjbar-Karami et al. (2014)	FIS	V_p, n, ρ,	0.89	Limestone, dolomites, anhydrites
Torabi-Kaveh et al. (2015)	ANN	V_p, ρ, n	0.96	Limestone
Armaghani et al. (2015)	ANFIS	ρ, V_p, Q, Pl	0.99	Granite
Armaghani et al. 2016)	ANN ICA-ANN	V_p, n, PLI, SHH	0.643 0.713	Granite
Madhubabu et al. (2016)	ANN	n, ρ, V_p, PLI, υ	0.96	Carbonate rocks
Ceryan (2016)	ANN LSSVM	V_{id}, n_e	0.809 0.860	Basalt, dacite, andesite, tuff
Atici (2016)	GEP	V_p, SHH, ρ, UCS	0.691	Marble, limestone, and magmatic rock
Behnia et al. (2017)	GEP	Q, n, ρ	0.927	Different type of rocks
Singh et al. (2017)	FIS, ANFIS,	V_p, n, ρ,	0.932	Basaltic rocks
Aboutaleb et al. (2018)	ANN SVR	υ_d, E_d	0.912 0.928	Limestone, marl, marl limestone, and marlstone
Roy and Singh (2018)	ANN, ANFIS	UCS, SP	0.97 0.98	Coal
Bejarbaneh et al. (2018)	FIS, ANN	SHH, PLI, V_P	0.689 0.819	Sandstone, shale, and mudstone
Rezaei (2018)	FIS	n, Hc, ρ, I_d	0.996	Clay shale, phyllite, sandstone, limestone shales, volcanic rocks
Umrao et al. (2018)	ANFIS	n, V_p, ρ	0.955	Sandstone, limestone
Ghasemi et al. (2018)	Mtr-M5P	SHH, V_p n, I_d, UW	0.87	Carbonate rocks
Matin et al. (2018)	RF	SHH, V_p	*0.93*	Travertine
Saedi et al. (2018)	ANFIS	n, BPI, TS, V_p, CPI	0.957	Migmatite
Mahdiabadi and Khanlari (2019)	ANN, ANFIS	BPI, CPI, PLI	0.782 0.789	Calcareous mudstones
Behzadafshar et al. (2019)	ANN GA-ANN	SHH, PLI, V_P	0.766 0.959	Granitic rocks

Table 1 (continued)

References	Technique	Input	R^2	Rock type
Mokhtari and Behnia (2019)	LLNF ANN COA-ANN	υ_d, ρ, n, V_p	0.962 0.703 0.980	Limestone
Tian et al. (2019)	ANN PSO-ANN ICA-ANN	V_p, SHH, PLI	0.753 0.943 0.952	Granite
Roy and Singh (2020)	ANN ANFIS	V_p, TS, τ	0.96 0.99	Coal, sandstone, shale
Rezaei 2020)	ANN	n, Hc, ρ, I_d, V_p, V_s, υ	0.981	Clay shale, phyllite, sandstone, limestone shales
Armaghani et al. (2020)	ANN GMDH	SHH, n, PLI, V_P	0.768 0.961	Granite
Acar and Kaya (2020)	LS-SVM	UW, V_P, PLL, TS	0.908	Tuffaceous rock
This study	SVR ANN GPR	n, V_p, I_d	0.695 0.859 0.898	Tuff, basalt, andesite, dacite, and granitic rocks with different degree of wethering

VBP the volumetric block proportion (%), *VBPr*$_i$ the volumetric different rock block proportion (%), ρ density, n porosity, n_e effective porosity, *UW* unit weight, *Vs* *P*-wave velocity, *Vp* *P*-wave velocity, *Vid* *P*-durability index, *WA* water absorption, *WC* water content, *SP* saturation pressure, *Hc* depth of coring, *Q* quartz content, *Pl* plagioclase content, *Mnrlgy* Minerology (Quartz, Feldspar, Detrital Clay, Other Minerals), *PrS* average particle size, *BD* bulk density, *VO* void ratio, *MPf* micropore fissure, pore wall, pore among particle), *BPI* block punch index, *CI* Cone indenter hardness, *CPI* the cylindrical punch index, *Id* slake durability index, *PLI* Point load index, *SHH* Schmidt hammer hardness, *SH* Shore hardness, *UCS* Uniaxial compressive strength, *TS* Tensile strength, τ shear strength, υ_d dynamic Poisson ratio, E_d dynamic the modulus of elasticity, *ANN* artificial neural network, *ANFIS* adaptive neuro-fuzzy inference system, *FIS* fuzzy inference system, *GA* genetic algorithm, *GE* genetic expression programming, *GP* genetic programming, *ICA* Imperialist Competitive Algorithm, *PSO* Particle Swarm Optimization, *GPR* Gaussian Process Regression, *GMDH* Group method of data handling, *MPRM* minimax probability machine regression, *SVM* support vector machine, *LS-SVM* least squares support vector machine, *RVM* relevance vector machine, *Mtr-M5P* 'Model trees and the M5P algorithm, *LLNF* local linear neuro-fuzzy, *COA-ANN* the hybrid cuckoo optimization algorithm-artificial neural network), *RF* random forests)

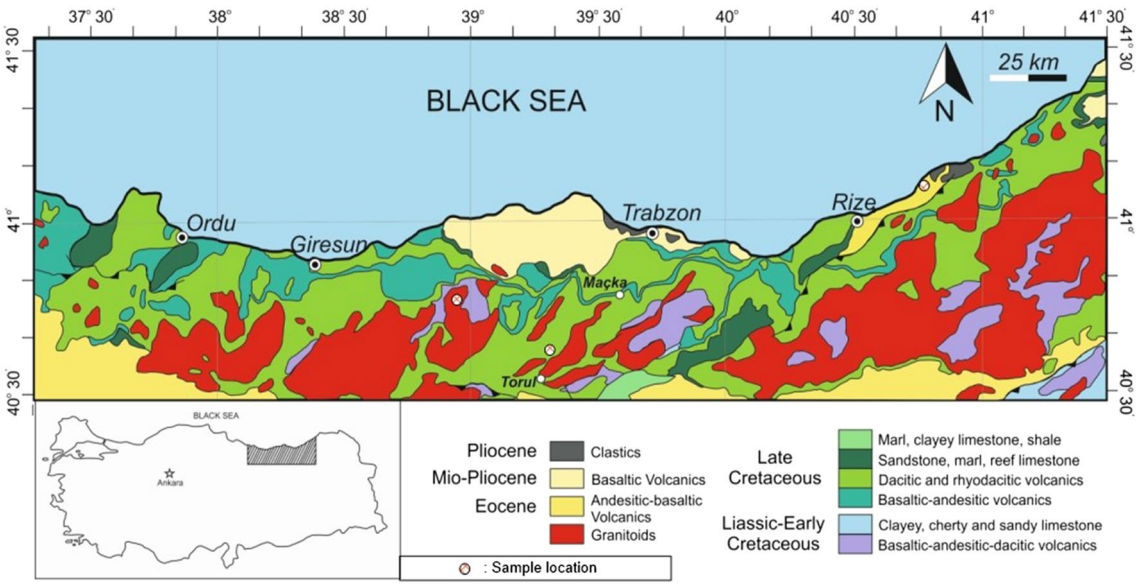

Fig. 1 Geology map of Eastern Pontides, NE Turkey, and location of the study area (Guven 1993; Hippolyte et al. 2017)

The samples were subjected to a four-cycle slake durability test to determine the slake durability index (Gokceoglu et al. 2000). This test was performed three times for each sample. The ultrasonic pulse velocity (UPV) test was conducted using the Portable Ultrasonic Non-destructive Digital Indicating Tester (PUNDIT®) without applying any pressure to the samples. The equipment generates an ultrasonic pulse with a frequency of 400 kHz and measures the transit time from the transmitter transducer through the sample to the receiving transducers. The time of ultrasonic pulses was read with an accuracy of 0.1 ms. The *P*-wave velocity of the rock samples without pores and fissures (V_m) was calculated using Eq. (2) (Barton 2007), and the *P*-durability index (V_{id}) is defined in Eq. (3) (Ceryan 2016)

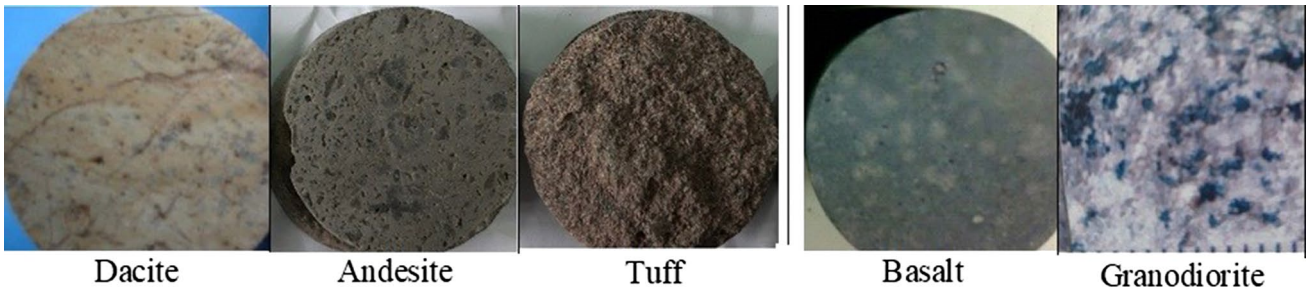

Fig. 2 Core samples investigated

$$\frac{1}{V_p} = \frac{\phi}{V_{\text{fl}}} + \frac{1-\phi}{V_{\text{m}}} \tag{2}$$

$$V_{\text{id}} = 0.01\ V_{\text{m}} I_d \tag{3}$$

where V_{fl} is the velocity in the fluid, ϕ is the ratio of the path length in the fluid to the total path length (the porosity), and I_d is the slake durability index.

To determine E_{s}, representing the sample stiffness against a uniaxial load, initially, the stress–strain curve for axial deformations was obtained for UCS. Then, E_{s} was defined as the slope of a line tangent to the stress–strain curve at a fixed percentage of the ultimate strength, 50%, for the test sample (Table 2).

Problem formulation

Methodology

The methodology for predicting the elastic modulus (E_{s}) is illustrated in Fig. 3. The flow chart consists of three main steps, which are (1) selection of inputs, (2) model development, and (3) model performance evaluation. In Step 1, the best subset regression approach was employed to determine inputs from the experimental study. The dataset was divided into two parts for the training (75% of the original data) and test (25% of the original data) sets of the regression models. In Step 2, the proposed regression models, namely, SVR, GPR, and ANN were developed using the training dataset. In Step 3, the developed regression models were validated using the test dataset. The statistical key performance indicators (KPIs), namely RMSE, NRMSE, R^2, MAE, NMAE, NS, VAF, AOC, Taylor diagram, the performance index with RMSE (PI_{RMSE}), and the performance index with MAE (PI_{MAE}), were applied in this step to evaluate the performances of the models.

Selection of inputs

The accuracy of the regression models largely depends on the type of function being used, as well as the quality and quantity of observed data. If there are more inputs than there should be, selecting a suitable set of inputs is necessary to reduce the noise resulting from unnecessary input data. Using suitable inputs, the interpretability of the model can be improved and the predictive ability increases (Omoruyi et al. 2019).

The input selection methods for the regression model can be collected under three main categories: (1) filter method (for example, Pearson's Correlation, Akaike information criterion, Bayesian information criterion, linear discriminant analysis, principal component analysis, analysis of variance, and chi-square), (2) embedded methods (for example, least angle and shrinkage selection operator and ridge regression), and (3) wrapper methods (for example, forward selection, backward elimination, recursive future elimination, stepwise method, best subset regression) (Huang et al. 2010; Desboulets 2018; Haque et al. 2018; Park and Klabjan 2020).

Here, the best subset regression approach was employed to determine the inputs. First, all possible regression models derived from all possible combinations of the inputs were defined. Then, the best model was determined according to KPIs, including Mean Square Error (MSE), RMSE, R^2, adjusted determination coefficient (adjR^2), and Mallow's C_p (Mallows and Sloane 1973), given in Eqs. (4)–(8).

$$\text{MSE} = \frac{1}{n-p}\sum_{i=1}^{n}\left(y_i - \hat{y}_i\right)^2 \tag{4}$$

$$\text{RMSE} = \sqrt{\text{MSE}} \tag{5}$$

$$R^2 = 1 - \frac{\text{MSE}_i}{\sigma^2} \tag{6}$$

Table 2 Lithology, index properties, and the modulus of elasticity (E_s) of the samples

Ex ID	Lty	SHH	n (%)	V_p (km/s)	I_d (%)	E_s (GPa)	V_m (km/s)	SHH × γ	V_{id} (km/s)
1	Anst	54	2.7	4.090	98.8	30.109	4.214	140.832	41.634
2	Dc	59	2.1	4.124	99.2	31.802	4.461	147.736	44.253
3	Anst	43	3.7	3.722	94.9	23.063	4.352	106.9	4.13
4	Tff	25	8.2	3.285	77.8	12.408	3.883	5.29	3.021
5	Tf	35	6.9	3.246	81.9	12.072	3.804	78.155	31.155
6	Tf	42	5	3.332	79.2	13.069	3.873	92.316	30.674
7	Anst	44	5.4	3.73	89.1	17.14	4.185	108.86	37.288
8	Dc	37	10.6	3.265	78.9	13.937	4.001	84.989	31.568
9	Grd	44	4.1	2.668	94.7	5.424	4.606	114.36	43.619
10	Grd	52	1.8	2.891	97.2	23.935	5.63	13.754	54.724
11	Bsl	42	1.5	3.896	93.8	24.835	4.239	105.34	39.762
12	Anst	38	4.1	3.691	95.4	25.891	4.09	97.394	39.019
13	Bsl	33	3.8	2.674	78.5	11.347	3.326	79.728	26.109
14	Dc	42	9.4	3.4	87.6	15.306	3.889	93.576	34.068
15	Dc	37	12.5	3.288	85.6	11.871	4.047	84.841	34.642
16	Grd	58	1.9	4.157	98.8	23.342	5.738	15.341	56.691
17	Bsl	52	1.1	4.202	98.1	26.752	4.332	136.14	42.497
18	Bsl	53	0.6	4.559	96.3	33.786	4.624	137.22	44.529
19	Dc	57	3.9	3.883	97.4	28.616	4.327	136.46	42.145
20	Grd	38	2.9	3.404	97.5	16.753	4.68	97.888	4.563
21	Dc	52	3.1	3.7	96.2	30.787	4.078	123.71	3.923
22	Dc	22	11.4	3.178	74.5	10.745	3.669	52.778	27.334
23	Grd	40	1.7	4.227	98.7	22.25	5.656	10.828	55.825
24	Grd	63	4	3.105	95.2	9.554	4.444	163.67	42.307
25	Dc	53	4.1	3.661	90.4	25.203	4.106	121.26	37.118
26	Dc	32	8.2	3.404	88.3	19.875	3.815	71.904	33.686
27	Anst	39	3	4.043	96.2	26.646	4.43	9.945	42.617
28	Grd	30	5.9	2.625	85.2	12.862	4.294	7.524	36.585
29	Dc	26	11.9	3.173	89.7	12.232	3.534	59.072	3.17
30	Dc	38	7.6	3.55	91.8	18.024	3.957	87.704	36.325
31	Tf	38	2.7	3.538	94.2	17.104	3.995	85.728	37.633
32	Dc	44	8.7	3.517	89.7	15.747	4.029	98.692	3.614
33	Anst	42	3.3	3.886	94.6	27.237	4.253	105.71	40.233
34	Grd	57	1.6	4.053	99.5	22.172	5.032	153.5	50.068
35	Dc	32	10.2	3.046	66.3	10.478	3.934	70.208	26.082
36	Dc	31	6.5	3.144	79.3	13.15	3.756	65.162	29.785
37	Grd	51	2.4	3.833	98.3	19.214	5.012	135	49.268
38	Grd	64	1.9	4.285	99.6	21.474	5.873	166.59	58.495
39	Tf	28	5.9	3.352	80.5	12.946	3.93	60.592	31.637
40	Grd	38	4.3	3.065	95.5	13.621	4.594	98.496	43.873
41	Dc	47	4.1	3.757	97.8	29.572	4.089	113.88	3.999
42	Dc	43	8.3	3.471	93.4	12.636	3.908	101.14	36.501
43	Dc	60	2.3	3.571	96.5	26.988	4.237	14.628	40.887
44	Dc	47	4.7	3.629	93.8	22.143	4.019	108.9	37.698
45	Bsl	37	2.9	3.057	88.7	17.12	3.682	90.798	32.659
46	Dc	42	4.7	3.836	93.7	24.035	4.274	99.834	40.047
47	Anst	50	3	4.1	96.3	28.374	4.16	12.985	40.061
48	Bsl	35	5.2	2.578	72.1	11.24	3.105	88.095	22.387
49	Bsl	39	2.8	3.575	94.7	22.435	3.985	98.397	37.738
50	Grd	34	1.7	3.504	97.5	17.084	4.95	91.324	48.263

Table 2 (continued)

Ex ID	Lty	SHH	n (%)	V_p (km/s)	I_d (%)	E_s (GPa)	V_m (km/s)	SHH × γ	V_{id} (km/s)
51	Dc	58	1.8	4.048	99.5	32.143	4.375	141.58	43.531
52	Dc	56	10.3	3.417	91.1	14.145	3.817	13.412	34.773
53	Dc	41	3.1	3.841	97.3	29.974	4.129	93.808	40.175
54	Dc	43	2.5	3.857	98.8	21.781	4.108	103.46	40.587
55	Bsl	48	0.7	4.625	98.6	36.458	4.747	123.55	46.805
56	Dc	33	10.6	2.876	68.4	7.025	3.381	74.382	23.126
57	Tf	32	6.9	3.246	81.6	13.327	3.993	70.272	32.583
58	Dc	48	5.8	3.479	94.5	16.783	3.876	119.57	36.628
59	Dc	38	8.1	3.228	74.9	9.829	3.886	92.834	29.106

Lty Anst, *Bsl* basalt, *Dc* dacite Grd: Tf, *SHH* Schmidt hammer hardness, SHH × γ =SHH × γ 10^{-2}, n porosity (%), V_p *P*-wave velocity (km/s), V_{id} *P*-durability index, V_m *P*-wave velocity in the solid part of the sample, I_d Slake durability index (%), E_s the modulus of elasticity (GPa)

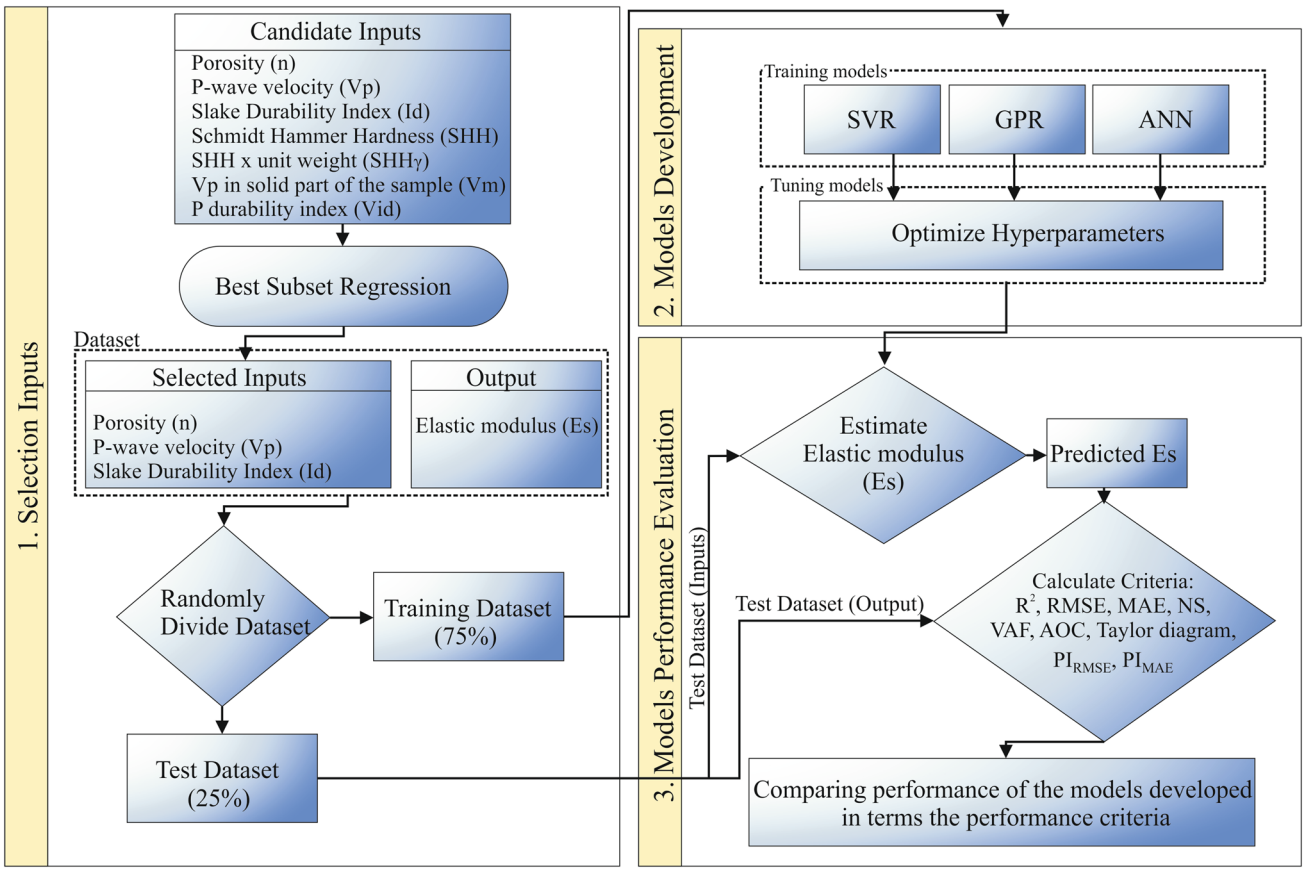

Fig. 3 The methodology of the present study for predicting the elastic modulus

$$\mathrm{Adj}R^2 = 1 - \frac{n-1}{n-i-1}\left(1-R^2\right) \tag{7}$$

$$C_p = (n-p)\frac{\mathrm{MSE}_i}{\mathrm{MSE}_F} - (n-2i-1) \tag{8}$$

where y_i and $\hat{y}_i$ are the measured and predicted values, respectively. MSE_i is the mean of residual squares in the model with i parameters, MSE_F is the mean of residual squares in the full model with p parameters, σ^2 is the variance of the dependent variable, n is the number of data, i is the number of inputs in the model, and p is the number of parameters in the aforementioned model.

R^2 increases with an increasing number of inputs, and therefore, it does not indicate the correct regression model. Instead, adjR^2 is generally considered to be a more accurate goodness-of-fit measure than R^2 because it applies a penalty score to the model when considering more inputs. The RSME is frequently used as a measure of the differences between the predicted and measured values. The performance of the model improves as the RMSE value decreases. The goal of Mallow's C_p is to achieve a balanced number of inputs in the model. It compares the precision and bias of the full model generated using all inputs to the models generated using a subset of inputs. The full model always yields a Mallow's C_p value equal to the number of parameters in the regression model (p), so the full model based on C_p should not be selected. Furthermore, a Mallow's C_p value below the p value represents sampling errors. If several models have Mallow's C_p near the p value, the model with the smallest value of the difference between the Mallow's C_p and the p value can be chosen as the best model.

The index properties, measured experimentally in this study, are: (1) Schmidt hammer hardness (SHH), (2) SHH $\times \gamma$ index, (3) slake durability index (I_d), (4) porosity (n), (5) P-wave velocity (V_p), (6) P-velocity in the solid part of the samples (V_m), and (7) P-durability index (V_{id}). These properties are also, the most frequently used inputs in the E_s prediction. The V_p and I_d values were measured experimentally, and the V_m and V_{id} values were calculated empirically from Eqs. (2) and (3). Therefore, the prediction models, namely, SVR, GPR, and ANN should be created by selecting only one of the V_m, V_{id}, and V_p values. Similarly, V_{id} and I_d cannot be used as inputs for the same prediction model at the same time. According to these defined conditions, the seven inputs were divided into three groups as follows: (1) n, V_p, I_d, SHH, and SHH $\times \gamma$, (2) n, V_{id}, SHH, and SHH $\times \gamma$, and (3) n, V_m, SHH, and SHH $\times \gamma$. Then, the best subset regression analysis was performed for each group to determine the inputs for the prediction models.

According to the results of the best subset regression analysis, the highest R^2 and adjR^2 values, as well as the lowest RSME value, for the linear regression model using the inputs in the second and third groups were 0.611, 0.575, and 4.930 MPa, respectively. However, the R^2, adjR^2, and RSME values for the linear regression model using the inputs of the first group were 0.774, 0.753, and 3.7635 MPa, respectively. Considering these values, the inputs in the first group, namely, n, V_p, I_d, SHH, and SHH $\times \gamma$ were selected to determine the optimum inputs that would be employed during the development of the prediction models.

Table 3 presents the results of the best subset regression analysis performed for different combinations of inputs from the first group and illustrates the two best-fitting models for each combination. The differences between Mallow's C_p and p value (the number of parameters in the full model) obtained for the 1st, 2nd, and 4th rows are larger than others. Although the smallest values of the differences between Mallow's C_p and the number of the parameters in the full model are obtained in the 7th and 9th rows, the input parameters in the 7th and 9th rows cannot be used because both SHH, and SHH $\times \gamma$ are used together in the regressions (Table 3). SHH, and SHH $\times \gamma$ are not independent of each other as SHH $\times \gamma$ is a function of R. The performance of the regression model in the 3rd row is slightly better than that of the model in the 8th row. In addition, while there are two inputs in the 3rd row, there are four inputs in the 8th row. Although the Mallow's C_p value obtained in the 3rd row is smaller than that in the 5th row, the R^2, adjR^2, RSME, and Mallow's $C_p - p$ values in the 5th row are better than those in the 3rd row (Table 3).

As a result of the best subset regression analysis, the regression in which porosity (n), P-wave velocity (V_p) and slake durability index (I_d) are used together yields the best performance. Thus, n, V_p, and I_d were employed as inputs for the regression models developed for the modulus of elasticity of the investigated samples.

Figure 4 illustrates the resulting histograms, cumulative distribution functions (CDFs), and additional statistical information, namely the number of data (N), maximum and minimum values, mean and standard deviations of both

Table 3 Best subset regression; E_s versus n, V_p, I_d, SHH and SHH $\times \gamma$

Row	Vars	R^2	adjR^2	RMSE (MPa)	Mallow's C_p	Mallow's C_p—p	n	V_p	I_d	SHH	SHH $\times \gamma$
1	1	0.674	0.668	4.3584	21.43	19.43		×			
2	1	0.490	0.481	5.4507	64.4	62.4			×		
3	2	0.743	0.734	3.8996	7.4	4.4	×	×			
4	2	0.714	0.704	4.1155	14.0	11.0		×	×		
5	3	0.748	0.735	3.8965	8.0	4.0	×	×	×		
6	3	0.744	0.730	3.9279	8.9	4.9	×	×		×	
7	4	0.764	0.747	3.8084	6.3	1.3	×	×		×	×
8	4	0.750	0.731	3.9229	9.7	4.7	×	×	×		×
9	5	0.774	0.753	3.7635	6.0	0	×	×	×	×	×

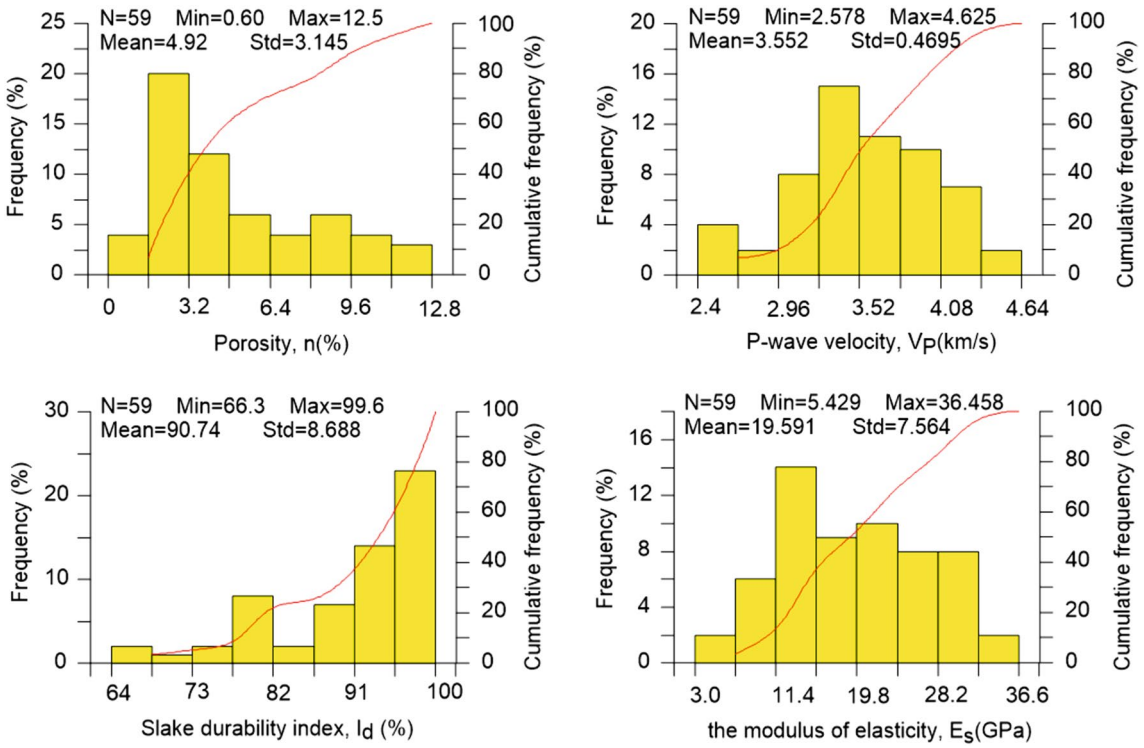

Fig. 4 Histograms and statistical summaries of porosity, *p*-wave velocity, slake durability index, and elastic modulus in the dataset

inputs (porosity, *p*-wave velocity, and slake durability index) and output (elastic modulus).

Most, if not all, machine learning algorithms, such as regression models, rely on selected training and test sets. These are often selected based on simple random sampling with prescribed ratios while considering that the training set should be larger than the test set. The experimental results (i.e. original dataset) are arbitrarily divided into two datasets that are the training dataset, which contains 75% of the original data, and the test dataset, which contains 25% of the original data. The training dataset was employed to fit the machine learning models, and the test dataset was used to evaluate the machine learning model fit based on the defined KPIs.

Regression model development

This study aims to develop reliable predictive models to determine the elastic modulus of magmatic rocks using porosity (n), *P*-wave velocity (V_p) and Slake durability index (I_d); and then, to compare the developed models utilizing the KPIs, the Performance Index, the REC curves, and Taylor diagram. Let us gather three inputs that are Porosity (n) (i.e. x_1), *P*-wave velocity $\left(V_p\right)$ (i.e. x_2), and the Slake durability index $\left(I_d\right)$ (i.e. x_3) in Eq. (9), where i and j are the index of experiments and inputs; whereas, N_i and N_j are the numbers of experiments and inputs, respectively.

$$\mathbf{X} = \left\{\mathbf{x_i}\right\} = \left\{x_{i,j}\right\} \quad \forall i = 1, \ldots, Ni \ , \quad \forall j = 1, \ldots, Nj \tag{9}$$

Similarly, let us gather the dependent variable E_s (i.e. y_1) in a set given in Eq. (10).

$$\mathbf{Y} = \left\{y_i\right\} \quad \forall i = 1, \ldots, Ni \tag{10}$$

In general, the regression models $\left(f\left(\mathbf{x_i}, \boldsymbol{\beta}\right)\right)$, between independent variables (inputs) and the dependent variables (targets/outputs), can be represented as follows:

$$\begin{aligned} &\hat{y}_i = f\left(\mathbf{x_i}, \boldsymbol{\beta}\right) + \epsilon_i \\ &\boldsymbol{\beta} = \left\{\beta_0, \beta_1, \ldots, \beta_j, \ldots, \beta_{Nj}\right\} \\ &\mathbf{x_i} = \left\{x_{i,1}, x_{i,2}, \ldots, x_{i,j}, \ldots, x_{i,Nj}\right\} \end{aligned} \tag{11}$$

where $(\boldsymbol{\beta})$ is the set of unknown parameters, and (ϵ) is the error term. One of the aims of this research is to develop

regression models that most closely fits the experimental results, and then evaluate and compare the performance of the developed regression models using defined KPIs. The background of the SVR, GPR, and ANN models are briefly explained in the following subsections.

Support vector regression

SVR model derived from statistical learning theory (Vapnik 1995) is used the sigmoid kernel function which is equivalent to a two-layer perceptron neural network. SVRs are alternative training methods for polynomial, radial basis function, and multilayer perceptron classifiers in which the weights of the network are found by solving a quadratic programming problem with linear constraints, rather than by solving a non-convex, unconstrained minimization problem as in standard ANN training (Huang et al. 2010).

The goal in linear regression is to minimize the error term between the actual and the predicted values of the dependent variables; whereas, the goal in SVR is to make sure that the errors do not exceed the threshold value (i.e. ε) (Suykens and Vandewalle 1999). Suppose that the empirical risk (ER) value is minimized, as follows:

$$\mathrm{ER} = \frac{1}{N}\sum_{i=1}^{Ni} |y_i - \hat{y}_i| \tag{12}$$

where $|y_i - \hat{y}_i|$ is ε-insensitive loss function written as:

$$|y_i - \hat{y}_i| = \begin{cases} 0 & \text{if } |y_i - \hat{y}_i| < \varepsilon \\ \left|y_i - f(\mathbf{x_i}, \boldsymbol{\beta}) - \varepsilon\right| - \varepsilon & \text{otherwise} \end{cases} \tag{13}$$

The proposed solution to this minimization problem is presented in Eq. (14).

$$\begin{aligned} \text{minimize } & \tfrac{1}{2}\boldsymbol{\beta}^T\boldsymbol{\beta} + C\sum_{i=1}^{Ni}\left(\xi_i + \xi_i^*\right) \\ & y_i - f(\mathbf{x_i}, \boldsymbol{\beta}) - \varepsilon \le \varepsilon + \xi_i \\ \text{subjec to } & f(\mathbf{x_i}, \boldsymbol{\beta}) + \varepsilon - y_i \le \varepsilon + \xi_i^* \\ & \xi_i, \xi_i^* \ge 0 \end{aligned} \tag{14}$$

where ξ_i, ξ_i^* are positive and negative slack variables from the threshold value (ε), respectively, and C is the meta-parameter which controls the trade between the model complexity (i.e. flatness) and the deviations from the (ε). If C is too large, the target only minimizes the empirical risk without considering model complexity in the optimization formulation. Additionally, the value of (ε) influences the number of support vectors used for constructing the regression function. The bigger the value (ε), the fewer support vectors are selected.

Gaussian process regression

GPR is a non-parametric kernel-based probabilistic regression model. Despite GPR is a powerful modeling tool, this method has been addressed in solving very few problems related to rock mechanics (Momeni et al. 2020; Kumar et al. 2013, 2014; Huang et al. 2017). The basic idea behind GPR is to predict the value of a function at a given point by computing a weighted average of the known values of the function in the neighborhood of the point. It combines a global model and local deviations (Rasmussen 2004; Hong et al. 2014). Now consider that the unseen observation, where the prediction will happen, $\mathbf{x}_* = \{x_{*,j}\} \quad \forall j = 1, \cdots, Nj$. The GPR model is of the form (Eq. 15)

$$\hat{y}(\mathbf{x}_*) = f(\mathbf{x}_*, \beta) + Z(\mathbf{x_i}, \mathbf{x_k}) \tag{15}$$

where $f(\mathbf{x}_*, \boldsymbol{\beta})$ is the unknown polynomial function, and $Z(\mathbf{x_i}, \mathbf{x_k})$ is the realization of a stochastic process with mean zero and nonzero covariance, which is given in Eq. (16).

$$\mathrm{cov}\left(Z(\mathbf{x_i}, \mathbf{x_k})\right) = \sigma^2\mathbf{R}\left(R(\mathbf{x_i}, \mathbf{x_k})\right) \tag{16}$$

where $\mathbf{R}$ is the correlation matrix, and $R(\mathbf{x_i}, \mathbf{x_k})$ is the correlation function between two observations (i.e. $\mathbf{x_i}, \mathbf{x_k}$). When the Gaussian correlation function is employed, the correlation function is expressed as:

$$R(\mathbf{x_i}, \mathbf{x_k}) = \exp\left[\sum_{j=1}^{Nj}\theta_j\left(x_{i,j} - x_{k,j}\right)\right] \quad \forall i, k = 1, \ldots, Ni \tag{17}$$

where θ_j is the unknown correlation parameter to be determined, and N_j is the number of inputs.

$$f(\mathbf{x}_*, \beta) = \hat{\boldsymbol{\beta}} + \mathbf{r^T}(\mathbf{x}_*)\mathbf{R}^{-1}\left(\mathbf{y} - \mathbf{f}\hat{\beta}\right) \tag{18}$$

where $\mathbf{y}$ is the column vector of length N_i that contains the responses of the experimental data and $\mathbf{f}$ is a column vector of length N_i that is filled with ones when $\mathbf{f}(\mathbf{x})$ is taken as a constant. $\mathbf{r^T}(\mathbf{x}_*)$ is the correlation vector between the unseen observation x_* and the whole seen observation (i.e.$\mathbf{X} = \{\mathbf{x_i}\} \quad \forall i = 1, \cdots, Ni$), which is defined as:

$$\mathbf{r^T}(\mathbf{x}_*) = \left[R(\mathbf{x}_*, \mathbf{x_1}), \ldots, R(\mathbf{x}_*, \mathbf{x_i}), \ldots, R(\mathbf{x}_*, \mathbf{x_{Ni}})\right]^T \tag{19}$$

The parameter $\hat{\beta}$ is calculated in Eq. (20).

$$\hat{\beta} = \left(\mathbf{f^T}\mathbf{R^{-1}}\mathbf{f}\right)^{-1}\mathbf{f^T}\mathbf{R^{-1}}\mathbf{y} \tag{20}$$

The estimated variance is calculated as:

$$\hat{\sigma}^2 = \frac{(\mathbf{y} - \mathbf{f}\beta)^T\mathbf{R}^{-1}(\mathbf{y} - \mathbf{f}\beta)}{N_i} \tag{21}$$

The unknown parameters θ_j in Eq. (21) obtained employing the maximum likelihood approached defined as:

$$\max \phi(\theta_j) = -\frac{N_i \ln\left(\hat{\sigma}^2\right) + \ln(|\mathbf{R}|)}{2} \tag{22}$$

Artificial neural network

ANN model is an alternative fitting method to map a relation between inputs and outputs. A neuron, which is the building blocks of ANN, is composed of the input layer, one or more hidden layers, and the output layer. Every neuron has connections, which are called weights, with every neuron in both the previous and the following layer. Moreover, each neuron has a bias that makes it work or not work depending on the level of the input signal (Agatonovic-Kustrin and Beresford 2000; Bektas et al. 2019a). The inter-connectivity between neurons is generally done either feed-forward (FFNN) and recurrent (RNN) architectures. In the presented work, a feed-forward hierarchical topology is used, and the neuron's output z can be expressed in Eq. (23).

$$z_j = \sum_{j=1}^{n} w_j x_j + \beta \tag{23}$$

where x_j is the input, w_j is the weight of the neuron, β is the bias value, and n is the number of the elements in inputs. The relationship between the output and the inputs is formulated as:

$$y_j = f_h(z_j) \tag{24}$$

where f_h is activation function which is generally linear and sigmoid. In the presented work, the sigmoid activation function was employed as defined in Eq. (25) (Ham and Kostanic 2000; Bektas et al. 2019b)

$$f_h = \frac{1}{1+e^{-x}} \tag{25}$$

The general network structure for a two-layer feedforward with a sigmoid transfer function (f_h) in the hidden layer and a linear transfer function (f_o) in the output is written in Eq. (26).

$$y_j = f_0\left(b + \sum_{h=1}^{n_h} w_h \cdot f_h\left(b_h + \sum_{i=1}^{n} w_{ih} \cdot x_{t-i}\right)\right) \tag{26}$$

Depending on the techniques used to train the feed-forward neural network models, different back-propagation algorithms have been developed. In this study, the Levenberg–Marquardt back-propagation algorithm was used for training. In the back-propagation phase, the performance index $E(W)$ to be minimized was defined as the sum of the squared errors between the target and network output as defined in Eq. (27).

$$E(W) = e^T e \tag{27}$$

where W consists of all weights in the network, and e is the error vector comprising the errors for all the training examples. When training with the Levenberg–Marquardt algorithm, the changing weights ΔW can be computed as follows:

$$\Delta W_k = -\left[J_k^T J_k + \mu_k I\right]^{-1} J_k^T e_k \tag{28}$$

Then, the update of the weights can be adjusted according to Eq. (29)

$$W_{k+1} = W_k + \Delta W_k \tag{29}$$

where J is the Jacobian matrix, I is the identity matrix, and μ is the Marquardt parameter to be updated using the decay rate β depending on the outcome. In particular, μ is multiplied by the decay rate β ($0<\beta<1$) when $E(W)$ decreases, while μ is divided by β when $E(W)$ increases in a new k-step. After the construction of the overall network, weights and biases parameters are iteratively adjusted to meet the predefined error criteria. Iteration by iteration the weights and the biases are updated proportionally to the mean squared error between the calculated output and the desired targets.

Criteria for the performance evaluation and data normalization

To justify the accuracies of the SVR, GPR, and ANN models, the following KPIs, namely, MSE, RMSE, R^2, adjR^2, MAE, the Nash–Sutcliffe coefficient (NS) to evaluate the capability of the model at simulating output data from the mean statistics, the variance account factor (VAF) to represent the ratio of the error variance to the measured data variance, and the Performance Index (PI), were computed for each model. MSE, RMSE, R^2, and adjR^2 were calculated using Eqs. (4)–(8). MAE, NS, and VAF were calculated using Eqs. (30)–(32), where y_i and $\hat{y}_i$ are the measured and predicted values. Here, the PI index is calculated separately according to both the normalized RMSE and normalized MAE values written in Eqs. (33) and (34). The NRMSE and NMAE values were obtained by dividing the RMSE and MAE values by the standard deviation of the E_s values measured.

$$\text{MAE} = \frac{1}{N_i}\sum_{t=1}^{N_i}\left|y_t - \hat{y}_t\right| \tag{30}$$

$$\mathrm{NS} = 1 - \frac{\sum_{t=1}^{N_i} \left(y_t - \hat{y}_t\right)^2}{\sum_{t=1}^{N_i} \left(y_t - \bar{y}_t\right)^2} \tag{31}$$

$$\mathrm{VAF}_i = \left(1 - \frac{\mathrm{var}\left(y_i - \hat{y}_i\right)}{\mathrm{var}\left(y_i\right)}\right) \cdot 100\% \tag{32}$$

$$\mathrm{PI}_{\mathrm{RMSE}} = \mathrm{adj}R^2 + 0.01\ \mathrm{VAF} - \mathrm{NRMSE} \tag{33}$$

$$\mathrm{PI}_{\mathrm{RMAE}} = \mathrm{adj}R^2 + 0.01\ \mathrm{VAF} - \mathrm{NMAE} \tag{34}$$

The Taylor diagram is also used to assess the performance of the regression models (Taylor 2001). It is a two-dimensional plot showing four statistical quantities: (1) the standard variation of observed data (σ_o), (2) the standard variation of predicted data (σ_p), (3) the correlation coefficient (R), and (4) the centered RMSE, which is the key to constructing the Taylor diagram, is defined Eq. (35).

$$\mathrm{RMSE}_{\mathrm{centered}} = \sigma_o^2 + \sigma_p^2 - 2\sigma_o\sigma_p R \tag{35}$$

The standard deviation shown in Fig. 5 is denoted by the radial distance from the origin. When the standard deviation of the predicted value (σ_p) is closer to the standard deviation of the observed (σ_o), the performance of the model is higher. R is represented by the azimuthal angle (Fig. 5). The centered RMSE is related to the distance between the observed (OBS) and developed model (MDL), assessed in units identical to those of the standard deviation. While the performance of the model increases with increasing R, it decreases with increasing centered RMSE value.

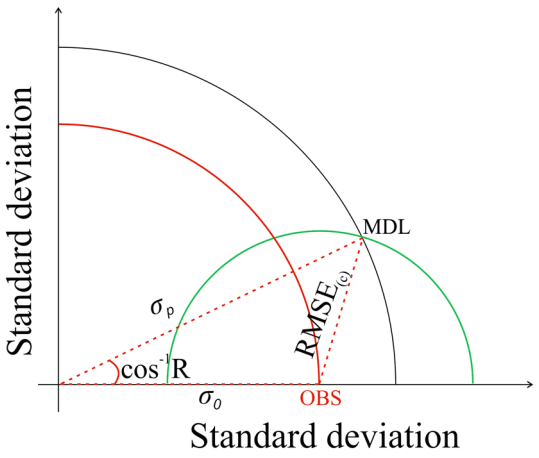

Fig. 5 Drawing of Taylor Diagram (reproduced from Taylor 2001)

Another graphical assessment of the performance of the models was conducted with the REC, which is a generalization of receiver operating characteristic (ROC) curves for regression (Bi and Bennett 2003). The REC curves plot the error tolerance on the x-axis versus the percentage of points predicted within the tolerance on the y-axis. The resulting curve estimates the cumulative distribution function of the error. The area over the REC curve (AOC) provides an approximation of the expected error. The AOC reveals additional information that can be used to assess the model. The smaller AOC, the better the model will perform (Bi and Bennett 2003).

The experimental results differ in scale. Therefore, an adjustment was made before employing the suggested methods to prevent the models from being dominated by variables with large values. Z-score normalization is widely used in this field, and its formulation is defined in Eq. (36).

$$\mathbf{x_i^{norm}} = \frac{x_{i,j} - \bar{\mathbf{x}}_\mathbf{i}}{\sqrt{\frac{1}{Nj}\sum_{j=1}^{Nj}\left(x_{i,j} - \bar{\mathbf{x}}_\mathbf{i}\right)^2}} \quad \forall j = 1, \ldots, Nj$$
$$\mathbf{X^{norm}} = \mathbf{x_i^{norm}} \quad \forall i = 1, \ldots, Ni \tag{36}$$

Results

Application and prediction

In this study, the SVR, GPR, and ANN models developed for the prediction of E_s were implemented in the MATLAB 2019a software environment. Considering the results of best subset regression, porosity (n), P-wave velocity (V_p) and slake durability index (I_d) were taken into account as input parameters in the models. The experimental results, that is, the original dataset, were randomly divided into two datasets, which were (1) the training dataset that contained 75% of the original data and (2) the test dataset that contained 25% of the original data.

In supervised machine learning, the covariance function (kernel function) expresses the statistical relationship between two data points (x_i, x_j). The kernel function ($k(x_i, x_j)$), which is specified by hyperparameters (θ), can be defined in various forms, such as Gaussian, exponential Gaussian, rational quadratic, Matern 5/2, and radial basis function. In this study, the MATLAB hyper-parameter optimization method was employed to obtain the optimum hyper-parameters for each regression model. For the SVR model, the Gaussian function was selected as the kernel and its hyper-parameters were optimized by the kernel scale method. The kernel scale, input means (μ), input standard

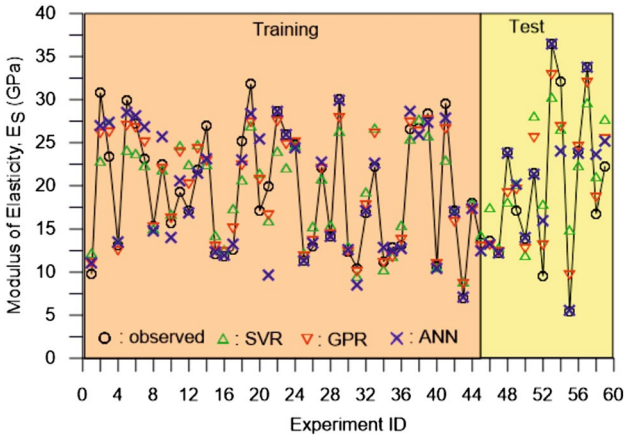

Fig. 6 Comparison of the estimated and measured E_s values

deviation (σ), and bias terms (β) were found to be 6.9, (4.9, 3.5, 90.73), (3.14, 0.46, 8.68), and 19.44, respectively. For the GPR model, the exponential Gaussian function was chosen as the kernel and its hyper-parameters were optimized by the sigma method. The characteristic length scale, input standard deviation, and bias term were computed as 9.29, 10.03, and 18.75, respectively. The Levenberg–Marquardt back-propagation approach was used to train a feedforward neural network using supervised learning. The constructed neural network was composed of one input layer with three neurons, two hidden layers with ten neurons in the 1st hidden layer and six neurons in the 2nd hidden layer, and an output layer with one neuron. The tansig function was a suitable function for smooth prediction in the ANN model and was thus used as a kernel function. The ANN model constructed was run for 300 iterations, and the best ANN model was selected according to the lowest MSE. Thirty-nine training epochs were used, and the 29th epoch was found to be the best, with an MSE of 1.678.

A comparison of the estimated values with the measured true values is shown in Figs. 6 and 7. Figure 6 indicates that the E_s values obtained from the ANN and GPR models are located closer to the measured values, compared to the values obtained for the SVR model. When considering the outputs of the regression line drawn according to the measured and predicted E_s values, and the line (1:1 line) where the measured and predicted values are equal (Fig. 7), the ANN and GPR model outputs are more successful than the other models.

Response surface

The training dataset was used to develop the regression models. The unseen values required for response surface plots were estimated using the developed models. The impacts of *P*-wave velocity and slake durability index with a constant porosity on E_s are depicted in Figs. 8, 9 and 10. According to all the regression models developed, E_s tends to increase with decreasing porosity, and with increasing *P*-wave velocity, and slake durability index. When the *n* value is kept constant, the E_s value increases as the V_p value increases. However, the change of E_s with I_d is not very clear. Moreover, when considering the plotted response surfaces, the SVR model shows linear behaviors, and the GPR model indicates quasi-linear behaviors, but the ANN model demonstrates completely nonlinear behaviors. Owing to the calculation algorithms of the SVR model, the response surfaces exhibit

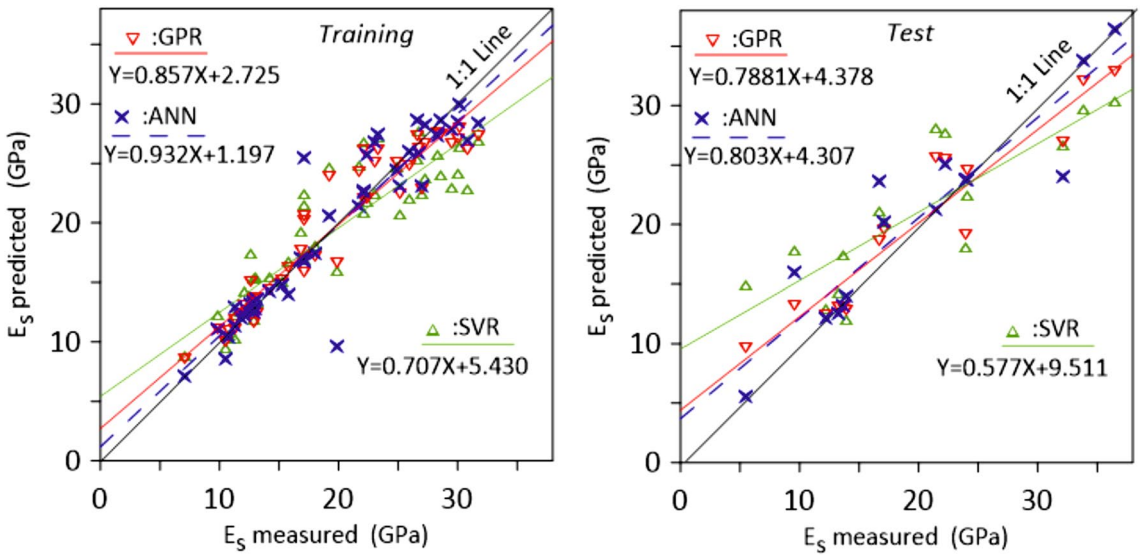

Fig. 7 Scatter plots for the SVR, GPR, and ANN models developed showing the training and test periods

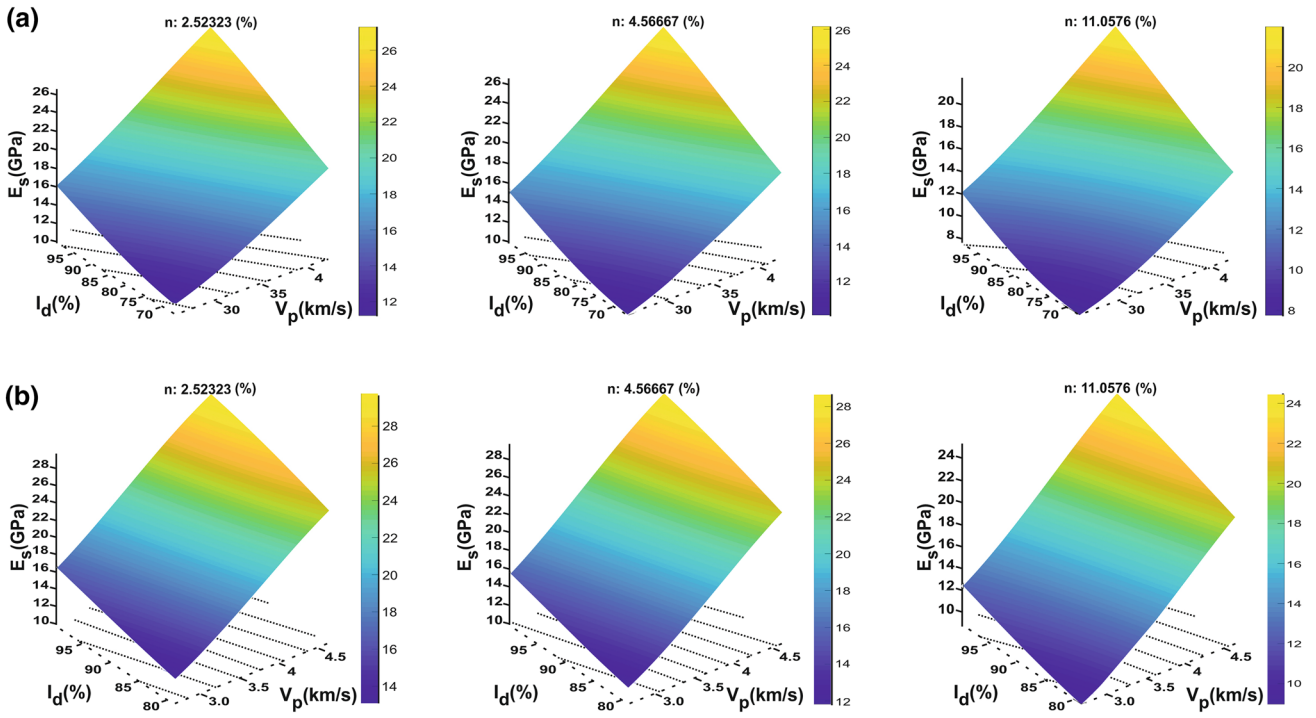

Fig. 8 Surface and contour plots for the SVR model showing the effect of I_d and V_p for selected n values on E_s; **a** training dataset and **b** test dataset

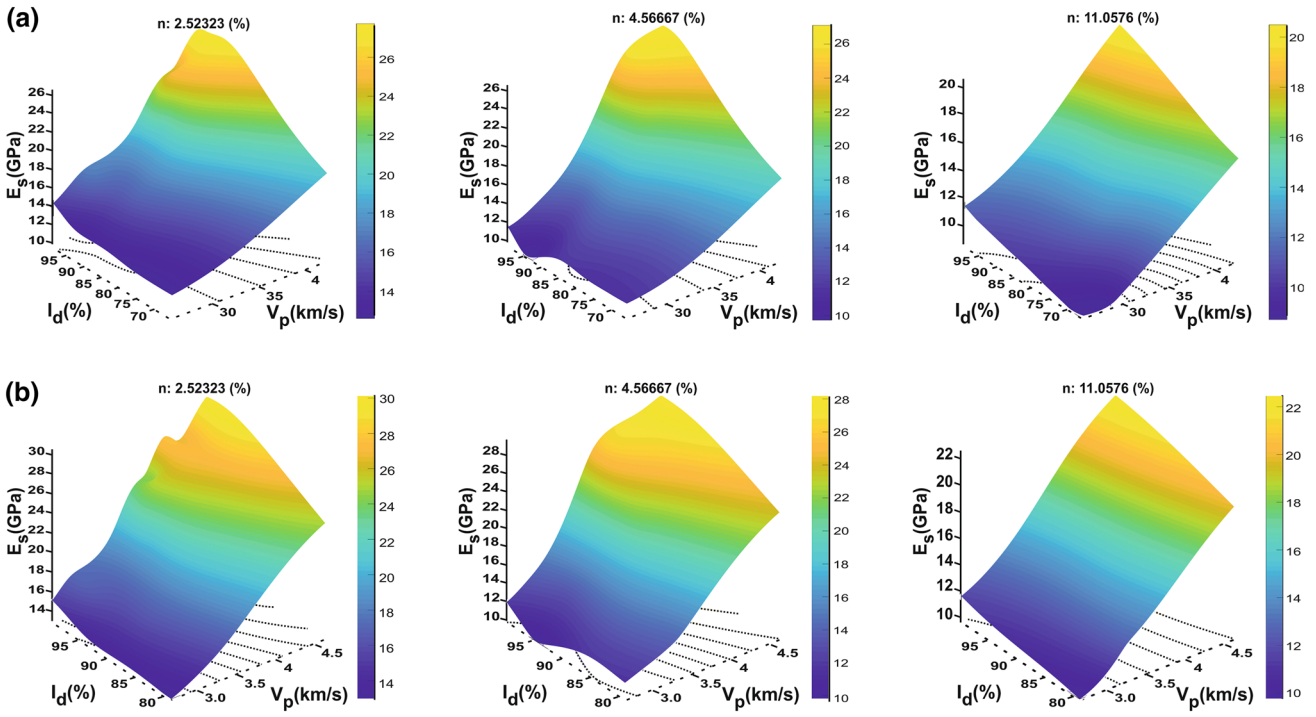

Fig. 9 Surface and contour plots for the GPR model showing the effect of I_d and V_p for selected n values on E_s; **a** training dataset and **b** test dataset

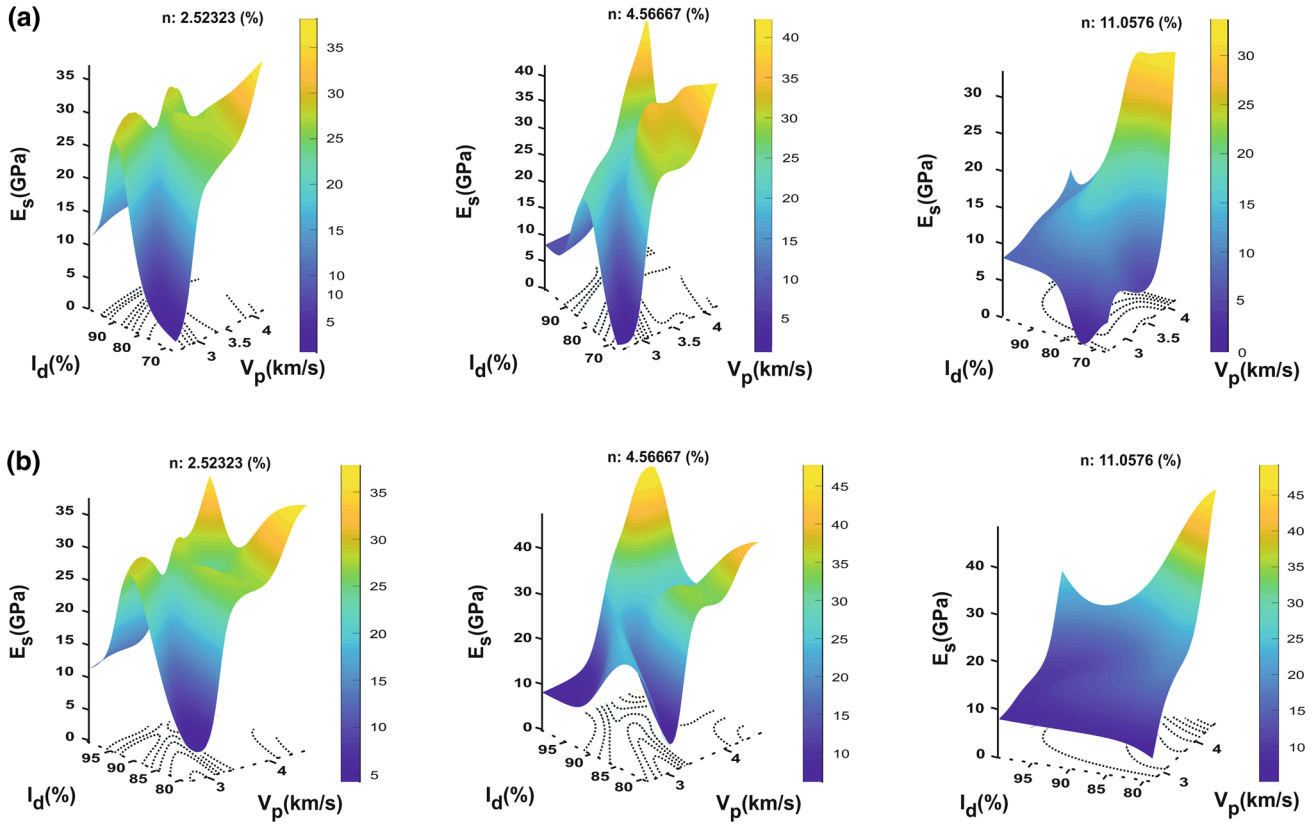

Fig. 10 Surface and contour plots for the ANN model showing the effect of I_d and V_p for selected n values on E_s; **a** training dataset and **b** test dataset

Table 4 Performance evaluation of the developed models using the defined KPIs

	RMSE (GPa)	MAE (GPa)	NRMSE	NMAE	R^2	adj R^2	NS	Min (GPa)	Max (GPa)	VAF (%)	PI_{RMSE}	PI_{MAE}
Training												
SVR	3.244	2.558	0.459	0.362	0.787	0.777	0.782	8.873	27.739	78.26	1.1008	1.1978
GPR	2.066	1.532	0.292	0.217	0.912	0.906	0.908	8.587	27.919	91.17	1.5251	1.6006
ANN	2.486	1.493	0.352	0.211	0.870	0.864	0.872	7.063	29.975	87.24	1.3844	1.5249
Observed								5.429	36.458			
Test												
SVR	5.662	5.196	0.619	0.568	0.695	0.644	0.615	11.990	30.355	62.71	0.6519	0.7029
GPR	3.365	3.043	0.368	0.332	0.898	0.881	0.864	9.666	32.928	86.52	1.3779	1.4142
ANN	3.767	2.337	0.412	0.255	0.859	0.835	0.830	5.512	36.406	83.39	1.2567	1.4139
Observed								7.028	31.802			

more linear behaviors compared to the GPR and ANN models. As shown in Fig. 9, the E_s value reaches its maximum at the maximum V_p value, regardless of the I_d value. This is because V_p plays an important role in estimating the E_s value in the ANN model. The response surfaces of the training and test data illustrate the same trends for each regression model.

Performance evaluation

In the training and test periods, the performance of the ANN model is very close to that of the GPR model, but there is a significant difference between the ANN and SVR models. This is also true for the SVR and GPR models (Table 4, Figs. 11 and 12).

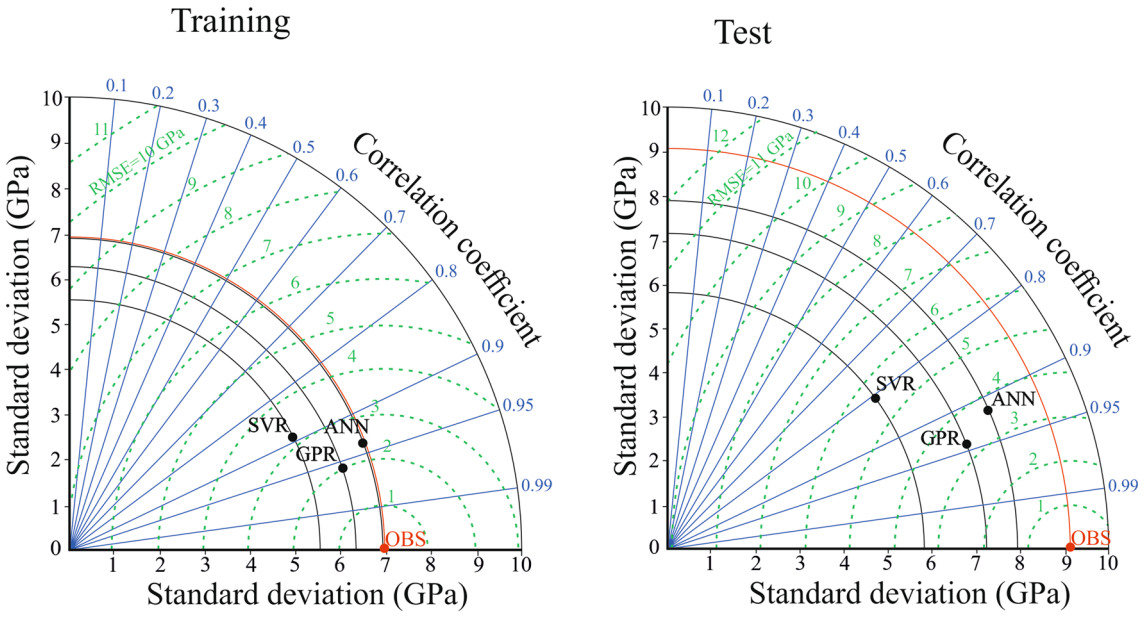

Fig. 11 Performance evaluation by Taylor diagram of the models developed

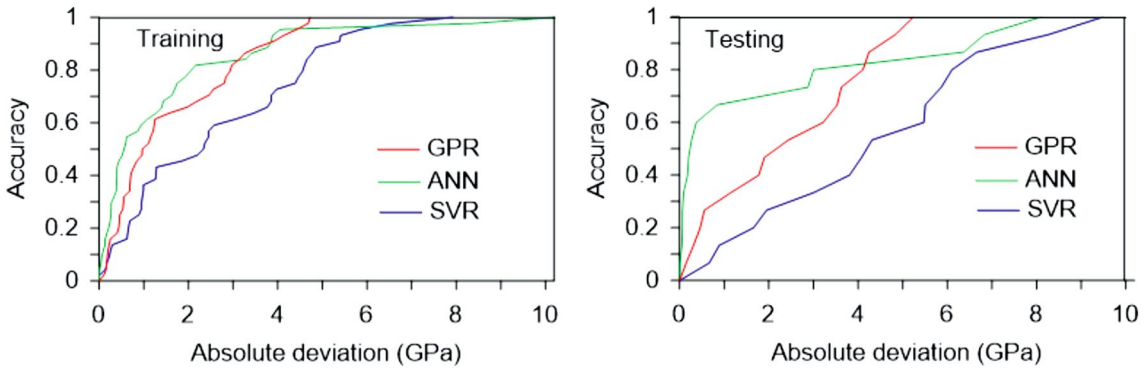

Fig. 12 ROC curves of the models developed

During the training period, the RMSE, NRMSE, MAE, NMAE R^2, NS, and VAF values for the SVR model were 3.244 GPa, 0.459, 2.558 GPa, 0.362, 0.787, 0.782, and 78.26%, respectively (Table 4). When considering the RMSE, the standard deviation of the E_s values estimated, and R values in the Taylor diagram, the performance of the SVR model is significantly worse than the performances of the ANN and GPR models (Fig. 11). The AOC value of the SVR model is 2.521 MPa (Fig. 12). The PI_{RMSE} and PI_{MAE} values obtained for the SVR model are 1.101 and 1.198, respectively (Table 4). From the performance indicators obtained for the SVR model, it can be concluded that the learning ability of the SVR model is insufficient.

During the training period, the RMSE, NRMSE, R^2, NS, and VAF values of the GPR model were 2.066 GPa, 0.292, 0.912, 0.908, and 91.17%, respectively, while the values for the ANN model were 2.486 GPa, 0.352, 0.870, 0.872, and 87.24%, respectively (Table 4). Additionally, the AOC, MAE, and NMAE values of the ANN model were 1.6846 GPa, 1.493 GPa, and 0.211, respectively, and were 2.377 GPa, 1.532, and 0.217, respectively, for the GPR model (Table 4 and Fig. 12). The standard deviation of the measured E_s was 7.0707 GPa, that of the predicted E_s GPa using the ANN model was 7.0673 GPa, and that of the predicted E_s using the GPR model was 6.3447. Therefore, the variability of the E_s values measured and that estimated by the ANN model are similar. The ANN model is more successful in terms of proximity to the measured E_s (Fig. 11). In addition, the best result for approaching the maximum and minimum values of E_s is obtained with the ANN model. However, as shown in the Taylor diagram (Fig. 11), the GPR model is more successful in terms of the RMSE and R values, than the

ANN model. In terms of the PI_{RMSE} and PI_{MAE} values, the GPR model performed better than the ANN model. While the PI_{RMSE} and PI_{MAE} values of the GPR model are 1.5251 and 1.6006, and those of the ANN model are 1.3844 and 1.5249, respectively.

For the test period, the RMSE, MAE, NRMSE, NMAE, R^2, NS, VAF, and AOC values of the SVR model are 5.662 GPa, 5.196 GPa, 0.619, 0.568, 0.695, 0.615, 62.7%, and 4.198 GPa, respectively (Table 4 and Fig. 12). The PI_{RMSE} and PI_{MAE} values obtained with the SVR model for the test data are 0.6519 and 0.7029, respectively. When considering the values of the key performance indices, the PI_{RMSE}, and PI_{MAE}, the SVR model is not successful in predicting the E_s of the samples investigated.

For the test data, the ANN and GPR models are better than the SVR model in terms of R, RMSE, proximity to the standard deviation of the measured E_s, and AOC values (Figs. 11 and 12).

The performance of the GPR model for the test data for R^2, RMSE, NRMSE, NS, and VAF is higher than that of the ANN model (Table 4). In the test period, the R^2, RMSE, NRMSE, NS, and VAF values obtained for the GPR model are 3.365 GPa, 0.368, 0.898, 0.864, and 86.5%, respectively, and those for the ANN model are 3.767 GPa, 0.412, 0.859, 0.835, and 83.4%, respectively (Table 4). When considering only the MAE, NMAE, and AOC values, the success of the ANN model in predicting E_s is higher than that of the GPR method. For the test period, the MAE, NMAE, and AOC values for the ANN model are 2.337 GPa, 0.255, and 1.3822 GPa, respectively, while those for the GPR model are 3.043 GPa, 0.332, and 1.5598 GPa, respectively (Table 4 and Fig. 12).

As illustrated in the Taylor diagram for the test data, the slope of the line connecting the point representing the GPR model with the origin is lower than the point representing the ANN model (Fig. 11). This indicates that the GPR model has a higher R value and a lower RMSE value than the ANN model in the test period. However, the point representing the ANN model is closer to the circle passing through the OBS (observed value) than the point representing the GPR model (Fig. 11). In the test period, the standard deviation of the measured E_s is 9.0517 GPa, while the standard deviations of E_s predicted using the ANN and GPR models are 7.637 GPa and 7.157 GPa, respectively. Therefore, for the test data, as for the training data, the variability of the measured E_s values and the variability of E_s values estimated by the ANN model are significantly closer to each other than that of the GPR model (Fig. 11). In the test period, the PI_{RMSE} and PI_{MAE} values obtained for the ANN model are 1.2567, and 1.4139, respectively, while those obtained for the GPR model are 1.3779 and 1.4142, respectively. When considering that PI_{RMSE} and PI_{MAE} were formed by more than one KPI, the GPR model performed better than the ANN model.

Discussion

To compare the performance of the models developed in this study to the prediction models given in the literature, the studies aimed to predict E_s of magmatic, and metamorphic rocks and include the prediction models based on ANN, SVR, and GPR models. As shown in Table 1, the properties of intact rock commonly used in the prediction models suggested for E_s of magmatic and metamorphic rocks are the Schmidt hammer hardness (SHH), shore hardness (SH), UCS, tensile strength (TS), point load index (PLI), and block punch index (BPI). Although the measurement of SHH is rapid and easily executed, simple, and portable, it has limitations, such as the anisotropy and heterogeneity of the rocks, a very small test conduction area, and surface roughness (Yilmaz 2009). UCS, TS, and BPI tests have two main limitations and problems, which are (1) a standard sample cannot always be obtained and (2) the tests cannot be repeatable. The BPI test is only valid for very thin small discs, and an irregular failure causes the need for a substantial amount of rock specimens (Yilmaz 2009). These limitations and problems related to the UCS, TS, and BPI are more concerning for weathered rocks. The disadvantages of PLI that do not need a standard sample are as follows: (1) tests are applied in very small areas, (2) invalid test results frequently occur, (3) the specimen may move during loading, and (4) micro-fissures may cross the conical platens (Yilmaz 2009). In addition, the force measurement accuracy in PLI may not be sufficient for the testing of weathered rock samples, and in these samples, there may be penetrating conical platens in the sample. The main shortcoming of the SH test is that the measurements are obtained from a random mineral, and anisotropy and/or heterogeneity of the rocks. Taking into account the limitations and problems, it can be acknowledged that there may be difficulties in using the results of such hardness and strength tests as inputs in the regression models.

The performances of the soft computing models to estimate the E_s of magmatic and metamorphic rock samples reported in Khandelwal and Singh (2011), Saedi et al. (2018), Tian et al. (2019), Armaghani et al. (2020), and Acar and Kaya (2020) are higher than those of the GPR model proposed in this study when comparing their R^2 values (Table 1). However, these prediction models use one or more of the SHH, SH, UCS, TS, PLI, and BPI as inputs. Other prediction models developed for the E_s of magmatic and metamorphic rock samples reported by Sonmez et al. (2006), Manouchehrian et al. (2013), Armaghani et al. (2016), Atici (2016), and Behzadafshar et al. (2019) also used hardness and strength properties as inputs, even though they had limitations and problems (Table 1). Furthermore, the performances of the regression models were not better

than those of the GPR and ANN models developed in this study.

Kumar et al. (2013) adopted a relevance vector machine (RVM), GPR, and minimax probability machine regression (MPMR) for the prediction of UCS and E_s of travertine samples. The GPR model in their study had a higher R^2 value than the GPR and ANN models developed in this study, but UCS and PLI were used as inputs in their study. The ANFIS models used by Armaghani et al. (2015) and Singh et al. (2017) performed better than the GPR models developed in this study but here, the GPR models were developed with different magmatic rock types with different degrees of weathering, while the ANFIS models were developed with only one rock type (Table 1). The input parameters of the LS-SVM models for predicting the E_s of weathered rock samples given in Ceryan (2016) are the effective porosity and the *P*-durability index. The *P*-durability index is based on the slake durability index and *P*-wave velocity. Although the LS-SVM model successfully predicted E_s, it had a lower R^2 value than the GPR and ANN models developed in this study. In addition, the *P*-durability index could not be selected as a suitable input parameter while selecting input parameters using the best subset regression analysis applied in this study. Behnia et al. (2017) developed a gene expression programming (GEP) model to predict the E_s and UCS of different rocks. The model used quartz content, porosity, and density as input parameters and performed successfully, with an R^2 value of 0.927. It can be concluded that using the GEP model to predict the E_s of weathered magmatic and metamorphic rock is useful.

When selecting inputs used in the suggested models in this study, the following factors were taken into account: (1) inputs are able to characterize these intrinsic characteristics and the state of weathering, (2) their measurements can be performed easily and rapidly in practical and economic terms, and (3) they provide high performance to the prediction models in which they are used. The simple and non-destructive properties (n, V_p, V_m, V_{id}, I_d, SHH, and SHH × γ) were obtained experimentally for use in the E_s estimation of the studied samples. As indicated in Table 1, these properties are the most frequently used inputs in prediction models. However, not all of them have been used in the same prediction models because of the practical and technical difficulties discussed here. For this, the best subset regression approach was employed to determine the inputs. As a result, porosity (n), *P*-wave velocity (V_p), and the slake durability index (I_d) were employed as inputs for the proposed SVR, GPR, and ANN models.

There are good relationships between the elastic wave velocity and the chemical and mineralogical composition of rocks (Ceryan 2015). This is also valid for weathered rock because the fresh mineral content decreases, while micro-fracture voids increase with weathering. Therefore, V_p decreases with increasing weathering (Ceryan et al. 2008a; Wyering et al. 2014; Momeni et al. 2017; de Vilder et al. 2019), and it is possible to characterize weathered magmatic and metamorphic rock material properties by V_p measurements (Ceryan et al. 2008b). Furthermore, it was also proposed that a non-destructive measurement of V_p offers an alternative input for E_s estimation with relative ease and at a low operational cost (Yasar and Erdogan 2004). The pore characteristics and fundamental microstructural parameters are important physical properties that govern the physical attributes of rocks, for example, strength, deformability, and hydraulic conductivity (Tugrul 2004). There are difficulties in determining pore size distribution, pore geometry, pore infilling, and pore connectivity, and therefore, porosity and effective porosity are commonly used to define the pores of rock materials (Ceryan 2014, 2015). The total porosity and the number of connected pores generally characterize the weathering state and these properties increase with weathering (Ceryan et al. 2008a). For these reasons, porosity or effective porosity is commonly used for estimating the E_s of rock materials (Table 1). The slake durability test is an inexpensive and easy test to conduct and requires very little sample preparation. Therefore, it is a good index for representing weathering processes (Lee and De Freitas 1989; Cargill and Shakoor 1990; Ceryan et al. 2008b; Sharma et al. 2008; Ceryan 2015). The slake durability index can be used inexpensively and easily to estimate the deformation modulus of weathered or soft rocks (Table 1). When the result of considering the best subset regression analysis performed, and the characterization of the weathering process in magmatic and metamorphic rocks, it is apparent that using porosity, slake durability index, and *P*-wave velocity as inputs in prediction models developed for rock materials is a practical and economical approach.

In all regression models, the combination of V_p and I_d can estimate the behavior of E_s referred to response surfaces illustrated in Figs. 7, 8, 9 and 10. Furthermore, the maximum E_s value is obtained at higher V_p and I_d values and lower n values as expected.

When the n value is kept constant, the E_s value enhances as the V_p value increases. On the other hand, the increase in the E_s value is very subtle only increasing with the I_d value when other inputs are held constant. For example, considering the same data point [V_p: 4.16 km/s, I_d: 99.5%] the E_s values are around 27 GPa with n: 2.52% for SVR, and GPR; whereas the E_s value is around 21 GPa with n: 11.057% for SVR, and GPR. Moreover, the estimated E_s value at the given data point for lower porosity value was around 27 GPa, but it decreased to around 12 GPa with the increase of the porosity value. As a result, ANN is more sensitive chances in V_p and n. On the other hand, the SVR and GPR models are more sensitive chances in V_p. As seen in the response surfaces, while the output values of the models are most

sensitive to the change of V_p, they are least sensitive to the change of I_d. The sensitivity of the output of the models in chances of the input parameters is related to the results of weathering processes on the rock material, as is related to the characteristics of soft computing techniques. Due to that the weathering product content, which having lower V_p than fresh minerals, and micro-fracture voids increase with weathering, the decreasing of V_p with weathering is more regularly and faster than I_d and n.

KPIs, namely VAF, RMSE, MAE, and R^2, can be separately used to examine model accuracy, but none are superior and therefore, the PI, which combines these KPIs, was suggested (Yagiz et al. 2012). Successively, adjR^2 was employed in computing the PI value instead of R^2 because it is a statistic with systematic error based on the number of independent variables in the equation, sample size, and the coefficient of variation (Ceryan 2014). However, the PI value given in Ceryan (2014) depends on the RMSE. The RMSE and MAE metrics, can range from 0 to ∞ and are indifferent to the direction of errors. The errors are squared before they are averaged, and therefore, the RMSE gives a relatively high weight to large errors. Owing to this characteristic of RMSE, it usually determines model performance differences better than other indices (Chai and Draxler and 2014). However, RMSE has important disadvantages because it is a function of three characteristics of a set of errors, rather than of one (the average error). RMSE varies with the variability within the distribution of error magnitudes, and the square root of the sample number, as well as with the average error magnitude (MAE) (Willmott and Matsuura 2005). Without the benefit of other information, for example, MAE, it is impossible to discern the extent to which RMSE reflects the central tendency (average error) or the variability within the distribution of squared errors (Mielke and Berry 2001; Willmott and Matsuura 2005; Willmott et al. 2009). Given the definition of MAE, it is clear that MAE, unlike RMSE, is an unambiguous measure of average error magnitude (Willmott and Matsuura 2005). However, the MAE might be affected by a large number of average error values without adequately reflecting some large errors (Chai and Draxler 2014). For these reasons, using the KPI, which considers both the errors themselves and the squares of the errors, would be more accurate. With this in mind, a new PI, PI_{MAE}, has been proposed using normalized MAE instead of normalized RMSE. Both PI_{RMSE} and PI_{MAE} were used in this study. When the values of these performance indices are less than 1, the prediction model fails, and the success of the model is higher as the value approaches 2. A prediction model is more successful if it has a larger PI_{RMSE} and PI_{MAE} value than the other model. If the PI_{RMSE} is large and the PI_{MAE} is small, other performance criteria should also be considered.

In this study, the REC diagram is drawn using the absolute value of errors (as in MAE). In contrast, RMSE is used in the Taylor diagram and does not provide the differences between the measured and obtained values directly. To overcome this deficiency, the REC curve was used to evaluate the performance of the models developed in this study.

Based on performance evaluation according to Performance Indexes, Taylor, and REC diagrams, it is clear that the SVR model developed in this study is the worst model for estimating the E_s of the investigated samples. In the training and test periods, the GPR model performs better than the ANN model in terms of the R and centered RMSE components of the Taylor diagram, while the variability (standard deviation) of E_s values obtained with the ANN model is closer to the variability of the observed E_s values. The AOC value obtained according to the absolute values of the errors (as in the MAE) is lower for the ANN model. However, the GPR model has a better performance than the ANN model in terms of PI_{RMSE} and PI_{MAE} values.

The SVR, GPR, and ANN models can approximate almost all types of non-linear functions, including quadratic functions. The soft computing models use a "black box" approach and have some difficulties in sharing the methodology with other researchers (Suykens and Vandewalle 1999; Agatonovic-Kustrin and Beresford 2000; Rasmussen 2004; Desai et al. 2008; Ahmadi and Rodehutscord 2017; Ozkat et al. 2017c). The SVR and GPR models are based on the same probabilistic regressive model, while ANN is not a probabilistic model. The GPR and SVR models developed here assume a Gaussian data distribution, but the ANN model does not assume any data distribution. The ANN and GPR models do not have a sparse solution. They use all sample/feature information to perform the prediction. The SVR model has the noteworthy advantage of frequently yielding sparse solutions. It minimizes reconstruction errors through convex optimization, ensuring that the optimal estimate is found, but it is not a unique solution. In the ANN model, the optimization is not always convex, and therefore, the solution is not always a global minimum (Suykens and Vandewalle 1999; Agatonovic-Kustrin and Beresford 2000; Rasmussen 2004; Khandelwal and Singh 2009; Kumar et al. 2013; Samui et al. 2019).

Parametric approaches distill knowledge about the training data into a set of numbers. They require a large amount of data, especially for architectures with many layers because of the vast number of weights and connections in ANN models. In contrast, Gaussian processes are non-parametric methods. A Gaussian processes kernel allows for the specification of a prior control on the function space, which can be extremely useful, especially when there are scant data (Bijl et al. 2017). However, as Gaussian processes are non-parametric, they need to take all the training data into account each time they make a prediction. This means that the computational cost of predictions increases with the

number of training samples (Agatonovic-Kustrin and Beresford 2000; Rasmussen 2004; Bijl et al. 2017).

The originality and limitations of this study are as follows:

The best subset regression approach was employed to determine the inputs in the proposed prediction model developed. As a result of this analysis, the most suitable parameters were found to be porosity (n), P-wave velocity (V_p), and the slake durability index (I_d). They are frequently used inputs in prediction models (Table 1) and are commonly used to define the state of weathering and in predicting the UCS and E_s of weathered magmatic and metamorphic rocks (Ceryan 2018). The measurements of V_p and n are non-destructive, repeatable, easy, and economical. The slake durability test is an inexpensive and easy test to conduct and requires very little sample preparation.

The ANN and GPR models developed in this study successfully predicted the E_s of the samples investigated. Although there are many ANN models to predict the E_s of rock materials, the number of GPR methods is quite low (Table 1). Moreover, according to the literature, there are very few soft computing models developed to assess the E_s of magmatic rock material with different degrees of weathering (Table 1). This study provides data and approaches to overcome this deficiency.

This study demonstrates that it is more useful to use together criteria based on the square of errors (e.g., RMSE and Taylor diagram) and criteria based on the absolute value of errors (i.e., MAE and REC have drawn depending on the absolute value of errors). In this study, the new Performance Index, PIMAE, which takes MAE into account, was created and it was stated that it would be beneficial to use together with this performance index and the Performance index based on RMSE. The ANN and GPR models given in this study have been developed to estimate the E_s of magmatic and metamorphic rock samples with different degrees of weathering. These models can be applied to magmatic and metamorphic rock samples containing at least three different degrees of weathering.

Conclusion

This study from NE Turkey, examined the applicability and capability of the SVR, GPR, and ANN models in E_s prediction of magmatic rocks with different degrees of weathering. The selection of the inputs for use in the models was performed using the best subset regression approach. As a result of these analyses, porosity, P-wave velocity, and the slake durability index that are used commonly in defining the weathering state and in predicting the E_s of weathered rocks, were selected as inputs for the prediction models developed in this study. Here, the weathering effect on the engineering behaviors of rock material is considered, and it is shown that using porosity, slake-durability index, and P-wave velocity together is a very powerful tool for estimating the elastic modulus of weathered magmatic and metamorphic rocks.

Given the difficulties of RMSE and MAE in expressing the error alone, it is useful to use both the index based on the absolute value of errors and the index based on the square value of error in evaluating the performance of the prediction models. For this, a new PI, PI_{MAE}, is proposed here, using normalized MAE instead of normalized RMSE.

According to the computed KPIs, Taylor diagram, and REC curves, it is concluded that the SVR model is insufficient for predicting the elastic modulus of the weathered magmatic rock samples. In the test period, the R^2, RMSE, and AOC values obtained for the SVR model were 0695, 5.662 GPa, and 4.198 GPa, respectively. In addition, the PI_{RMSE} and PI_{MAE} obtained for the SVR model developed were lower than 1.0, being 0.6519 and 0.7028, respectively.

During the training and test periods, the results of the performance analysis of the ANN and GPR models using KPIs, the Taylor diagram, and the REC curves were excellent. In both the training and test periods, when the performance metrics were considered one by one, in the criteria based on the absolute value of error, for example, MAE, NMAE, and AOC, and when approaching extreme measured values and standard deviation of E_s value, the ANN model was more successful than the GPR model. The MAE, NMAE, and AOC values of the ANN model for the test data were 2.337 GPa, 0.255, and 1.3822 GPa, respectively, while those of the GPR model were 0.043, 0.332, and 1.5598 GPa, respectively. Conversely, in terms of R^2, RMSE, NRMSE, NS, and VAF, the GPR model performed better than the ANN model. In the test period, the R^2 value obtained for the GPR model was 0.898, while that for the ANN model was 0.859. For PI_{RMSE} and PI_{MAE}, which were created by combining multiple KPIs, the performance of the GPR model was better than that of the ANN model. The PI_{RMSE} and PI_{MAE} values of the GPR model for the test data were 1.3779 and 1.4142, respectively, while those for the ANN model were 1.2567 and 1.4139, respectively. In the Taylor diagram, the GPR model performed better than the ANN model. Moreover, because of the probabilistic and non-parametric nature of the GPR system, it can be easily simulated and projected.

The performance of the GPR model is slightly better than that of the ANN model, although both the models are successful in predicting the E_s of the magmatic rock samples with different degrees of weathering. It would be useful to develop GPR and ANN models with porosity, P-wave velocity, and the slake durability index to predict the E_s and UCS of other weathered rock samples, including samples with at least three different degrees of weathering.

Acknowledgements The authors declare that they have no known competing financial interests or personal relationships that could have appeared to influence the work reported in this manuscript. The manuscript has included data and is given as electronic supplementary data.

Author contributions Not applicable.

Funding Not applicable.

Availability of data and material The manuscript has included data and is given as electronic supplementary data.

Code availability Not applicable.

Declarations

Conflict of interest The authors declare that they have no known competing financial interests or personal relationships that could have appeared to influence the work reported in this manuscript.

References

Aboutaleb S, Behnia M, Bagherpour R, Bluekian B (2018) Using non-destructive tests for estimating uniaxial compressive strength and static Young's modulus of carbonate rocks via some modeling techniques. Bull Eng Geol Environ 77:1717–1728. https://doi.org/10.1007/s10064-017-1043-2

Acar MC, Kaya B (2020) Models to estimate the elastic modulus of weak rocks based on least square support vector machine. Arab J Geosci 13:1–12. https://doi.org/10.1007/s12517-020-05566-6

Agatonovic-Kustrin S, Beresford R (2000) Basic concepts of artificial neural network (ANN) modeling and its application in pharmaceutical research. J Pharm Biomed Anal 22:717–727. https://doi.org/10.1016/S0731-7085(99)00272-1

Ahmadi H, Rodehutscord M (2017) Application of artificial neural network and support vector machines in predicting metabolizable energy in compound feeds for pigs. Front Nutr 4:27. https://doi.org/10.3389/fnut.2017.00027

Ajalloeian R, Mansouri H, Baradaran E (2017) Some carbonate rock texture effects on mechanical behavior, based on Koohrang tunnel data. Iran Bull Eng Geol Environ 76:295–307. https://doi.org/10.1007/s10064-016-0861-y

Alemdag S, Gurocak Z, Cevik A, Cabalar AF, Gokceoglu C (2016) Modeling deformation modulus of a stratified sedimentary rock mass using neural network, fuzzy inference and genetic programming. Eng Geol 203:70–82. https://doi.org/10.1016/j.enggeo.2015.12.002

Alikarami R, Torabi A, Kolyukhin D, Skurtveit E (2013) Geostatistical relationships between mechanical and petrophysical properties of deformed sandstone. Int J Rock Mech Min Sci 63:27–38. https://doi.org/10.1016/j.ijrmms.2013.06.002

Armaghani DJ, Tonnizam Mohamad E, Momeni E, Narayanasamy MS, Amin MFM (2015) An adaptive neuro-fuzzy inference system for predicting unconfined compressive strength and Young's modulus: a study on main range granite. Bull Eng Geol Environ 74:1301–1319. https://doi.org/10.1007/s10064-014-0687-4

Armaghani DA, Mohamad TE, Momeni E, Monjezi M, Narayanasamy MS (2016) Prediction of the strength and elasticity modulus of granite through an expert artificial neural network. Arab J Geosci 9:48. https://doi.org/10.1007/s12517-015-2057-3

Armaghani DJ, Momeni E, Asteris P (2020) Application of group method of data handling technique in assessing deformation of rock mass. Metaheuristic Comput Appl 1:1–18. https://doi.org/10.12989/mca.2020.1.1.001

Atici U (2016) Modelling of the elasticity modulus for rock using genetic expression programming. Adv Mater Sci Eng 8:45. https://doi.org/10.1155/2016/2063987

Aufmuth RE (1974) A systematic determination of engineering criteria for rock (No. CERL-TR-M-799 Final Rept)

Barton N (2007) Fracture-induced seismic anisotropy when sharing is induced in production from fractured reservoirs. J Seism Explor 16:115

Behnia D, Behn M, Shahriar K, Goshtasbi K (2017) A New predictive model for rock strength parameters utilizing GEP method. Proc Eng 191:591–599. https://doi.org/10.1016/j.proeng.2017.05.222

Behzadafshar K, Sarafraz ME, Hasanipanah M, Mojtahedi Tahir MM (2019) Proposing a new model to approximate the elasticity modulus of granite rock samples based on laboratory tests results. Bull Eng Geol Environ 78:527–1536. https://doi.org/10.1007/s10064-017-1210-5

Beiki M, Majdi A, Givshad AD (2013) Application of genetic programming to predict the uniaxial compressive strength and elastic modulus of carbonate rocks. Int J Rock Mech Min Sci 63:159–169. https://doi.org/10.1016/j.ijrmms.2013.08.004

Bejarbaneh BY, Bejarbaneh EY, Amin MFMl, (2018) Intelligent modelling of sandstone deformation behaviour using fuzzy logic and neural network systems. Bull Eng Geol Environ 77:345–361. https://doi.org/10.1007/s10064-016-0983-2

Bektas O, Jones JA, Sankararaman S, Roychoudhury I, Goebel K (2019a) A neural network framework for similarity-based prognostics. MethodsX 6:383–390. https://doi.org/10.1016/j.mex.2019.02.015

Bektas O, Jones JA, Sankararaman S, Roychoudhury I, Goebel K (2019b) A neural network filtering approach for similarity-based remaining. Int J Adv Manuf Technol 101:87–103. https://doi.org/10.1007/s00170-018-2874-0

Bi J, Bennett KP (2003) Regression error characteristic curves. In: Proceedings of the 20th international conference on machine learning (ICML-03), pp 43–50

Bidgoli MN, Zhao Z, Jing L (2013) Numerical evaluation of strength and deformability of fractured rocks. J Rock Mech Geotech Eng 5(2013):419–430. https://doi.org/10.1016/j.jrmge.2013.09.002

Bijl H, Schön TB, van Wingerden J-W, Michel Verhaegen M (2017) System identification through online sparse Gaussian process regression with input noise. IFAC J Syst Control 2:1–11. https://doi.org/10.1016/j.ifacsc.2017.09.001

Brotons V, Tomás R, Ivorra S, Grediaga A, Martínez-Martínez J, Benavente D, Gómez-Heras M (2016) Improved correlation between the static and dynamic elastic modulus of different types of rocks. Mater Struct Constr. https://doi.org/10.1617/s11527-015-0702-7

Cargill JS, Shakoor A (1990) Evaluation of empirical methods for measuring the uniaxial compressive strength of rock. Int J Rock Mech Min Sci 27:495–503. https://doi.org/10.1016/0148-9062(90)91001-N

Ceryan N (2014) Application of support vector machines and relevance vector machines in predicting uniaxial compressive strength of volcanic rocks. J African Earth Sci. https://doi.org/10.1016/j.jafrearsci.2014.08.006

Ceryan S (2015) New weathering indices for evaluating durability and weathering characterization of crystalline rock material: a case study from NE Turkey. J Afr Earth Sci 103:54–64. https://doi.org/10.1016/j.jafrearsci.2014.12.005

Ceryan N (2016) A review of soft computing methods application in rock mechanic engineering. Handbook of research on advanced

computational techniques for simulation-based engineering. IGI Global, pp 1–70
Ceryan S (2018) Weathering indices used in evaluation of the weathering state of rock material. In: Ceryan N (ed) Handbook of research on trends and digital advances in engineering geology, Chap 4. IGI Global United States of America, pp 132–186
Ceryan S, Tudes S, Ceryan N (2008a) A new quantitative weathering classification for igneous rocks. Environ Geol 55:1319. https://doi.org/10.1007/s00254-007-1080-4
Ceryan S, Tudes S, Ceryan N (2008b) Influence of weathering on the engineering properties of Harsit granitic rocks (NE Turkey). Bull Eng Geol Environ 67:97–104. https://doi.org/10.1007/s10064-007-0115-0
Chai T, Draxler TT (2014) Root mean square error (RMSE) or mean absolute error (MAE)?—arguments against avoiding RMSE in the literature. Geosci Model Dev 7:1247–1250. https://doi.org/10.5194/gmd-7-1247-2014
de Vilder SJ, Brain MJ, Rosser NJ (2019) Controls on the geotechnical response of sedimentary rocks to weathering. Earth Surf Process Landf 44:1910–1929. https://doi.org/10.1002/esp.4619
Deere DU, Miller RP (1966) Engineering classification and index properties for intact rock. Illinois Univ At Urbana Dept Of Civil Engineering
Dehghan S, Sattari G, Chehreh CS, Aliabadi MA (2010) Prediction of uniaxial compressive strength and modulus of elasticity for Travertine samples using regression and artificial neural networks. Min Sci Technol. https://doi.org/10.1016/S1674-5264(09)60158-7
Desai KM, Survase SA, Saudagar PS et al (2008) Comparison of artificial neural network (ANN) and response surface methodology (RSM) in fermentation media optimization: case study of fermentative production of scleroglucan. Biochem Eng J 41:266–273. https://doi.org/10.1016/j.bej.2008.05.009
Desboulets LDD (2018) A review on variable selection in regression analysis. Econometrics 6:45. https://doi.org/10.3390/econometrics6040045
Diamantis K, Gartzos E, Migiros G (2014) Influence of petrographic characteristics on physico-mechanical properties of ultrabasic rocks from central Greece. Bull Eng Geol Environ 73:1273–1292. https://doi.org/10.1007/s10064-014-0584-x
Dinçer I, Acar A, Çobanoğlu I, Uras Y (2004) Correlation between Schmidt hardness, uniaxial compressive strength and Young's modulus for andesites, basalts and tuffs. Bull Eng Geol Environ 63:141–148. https://doi.org/10.1007/s10064-004-0230-0
Erguler ZA, Ulusay R (2009) Water-induced variations in mechanical properties of clay-bearing rocks. Int J Rock Mech Min Sci 46:355–370. https://doi.org/10.1016/j.ijrmms.2008.07.002
Fener M, Kahraman S, Bilgil A, Gunaydin O (2005) A comparative evaluation of indirect methods to estimate the compressive strength of rocks. Rock Mech Rock Eng 38:329–343. https://doi.org/10.1007/s00603-005-0061-8
Ghasemi E, Kalhori H, Bagherpour R, Yagiz S (2018) Model tree approach for predicting uniaxial compressive strength and Young's modulus of carbonate rocks. Bull Eng Geol Environ 77:331–343. https://doi.org/10.1007/s10064-016-0931-1
Gokceoglu C, Zorlu K (2004) A fuzzy model to predict the uniaxial compressive strength and the modulus of elasticity of a problematic rock. Eng Appl Artif Intell 17:61–72. https://doi.org/10.1016/j.engappai.2003.11.006
Gokceoglu C, Ulusay R, Sonmez H (2000) Factors affecting the durability of selected weak and clay-bearing rocks from Turkey, with particular emphasis on the influence of the number of drying and wetting cycles. Eng Geol 57:215–237. https://doi.org/10.1016/S0013-7952(00)00031-4
Guven IH (1993) Geological and metallogenic map of the eastern black sea region; 1: 250000 Map. Publications of Mineral Research and Exploration General Directorate of Turkey
Ham FM, Kostanic I (2000) Principles of neurocomputing for science and engineering. McGraw-Hill Higher Education, p 672 (**ISBN:978-0-07-025966-9**)
Haque MM, Rahman A, Hagare D, Chowdhury RK (2018) A comparative assessment of variable selection methods in urban water demand forecasting. Water 10:419. https://doi.org/10.3390/w10040419
Heap MJ, Lavallée Y, Petrakova L et al (2014) Microstructural controls on the physical and mechanical properties of edifice-forming andesites at Volcán de Colima, Mexico. J Geophys Res Solid Earth 119:2925–2963. https://doi.org/10.1002/2013JB010521
Heidari M, Khanlari GR, Momeni AA (2010) Prediction of elastic modulus of intact rocks using artificial neural networks and nonlinear regression methods. J Appl Sci Res 4:5869–5879
Hippolyte JC, Müller C, Sangu E, Kaymakci N (2017) Stratigraphic comparisons along the Pontides (Turkey) based on new nannoplankton age determinations in the Eastern Pontides: geodynamic implications. Geol Soc Spec Publ 428:323–358. https://doi.org/10.1144/SP428.9
Hoek E, Diederichs MS (2006) Empirical estimation of rock mass modulus. Int J Rock Mech Min Sci 36:203–215. https://doi.org/10.1016/j.ijrmms.2005.06.005
Hong X, Gao J, Jiang X, Harris CJ (2014) Estimation of Gaussian process regression model using probability distance measures. Syst Sci Control Eng 1:655–663. https://doi.org/10.1080/21642583.2014.970731
Huang Y, Lan Y, Thomson SJ, Fang A, Hoffmann WC, Lacey RE (2010) Development of soft computing and applications in agricultural and biological engineering. Comput Electron Agric 71(2):107–127. https://doi.org/10.1016/j.compag.2010.01.001
Huang XB, Zhang Q, Zhu HH, Zhang LY (2017) An estimated method of intact rock strength using gaussian process regression. In: 51st US rock mechanics/geomechanics symposium. American Rock Mechanics Association
International Society for Rock Mechanics (2007) The complete ISRM suggested methods for rock characterization, testing and monitoring: 1974–2006. In: Ulusay H (ed) Suggested methods prepared by the commission on testing methods. International Society for Rock Mechanics, p 628
Kahraman S, Gunaydin O, Alber M, Fener M (2009) Evaluating the strength and deformability properties of Misis fault breccia using artificial neural networks. Expert Syst Appl 36:6874–6878. https://doi.org/10.1016/j.eswa.2008.08.002
Karakus M, Kumral M, Kilic O (2005) Predicting elastic properties of intact rocks from index tests using multiple regression modelling. Int J Rock Mech Min Sci 42:323–330. https://doi.org/10.1016/j.ijrmms.2004.08.005
Kayabasi A, Gokceoglu C, Ercanoglu M (2003) Estimating the deformation modulus of rock masses: a comparative study. Int J Rock Mech Min Sci 40:55–63. https://doi.org/10.1016/S1365-1609(02)00112-0
Khandelwal M, Singh TN (2009) Correlating static properties of coal measures rocks with *P*-wave velocity. Int J Coal Geol 79:55–60. https://doi.org/10.1016/j.coal.2009.01.004
Khandelwal M, Singh TN (2011) Predicting elastic properties of schistose rocks from unconfined strength using intelligent approach. Arab J Geosci 4:435–442. https://doi.org/10.1007/s12517-009-0093-6
Kim E, Stine MA, de Oliveira DBM, Changani H (2017) Correlations between the physical and mechanical properties of sandstones with changes of water content and loading rates. Int J Rock Mech

Min Sci 100:255–262. https://doi.org/10.1016/j.ijrmms.2017.11.005

Ko J, Jeong S, Lee JK (2016) Large deformation FE analysis of driven steel pipe piles with soil plugging. Comput Geotech 71:82–97. https://doi.org/10.1016/j.compgeo.2015.08.005

Kumar M, Samui P, Naithani AK (2013) Determination of uniaxial compressive strength and modulus of elasticity of travertine using machine learning techniques. Int J Adv Soft Comput Appl 54:1–13

Kumar M, Bhatt MR, Samui P (2014) Modeling of elastic modulus of jointed rock mass: Gaussian process regression approach. Int J Geomech 14:06014001. https://doi.org/10.1061/(ASCE)GM.1943-5622.0000318

Kurtuluş C, Irmak TS, Sertçelik I (2010) Physical and mechanical properties of Gokceada: Imbros (NE Aegean Sea) island andesites. Bull Eng Geol Environ 69:321–324. https://doi.org/10.1007/s10064-010-0270-6

Lee SG, De Freitas MH (1989) A revision of the description and classification of weathered granite and its application to granites in Korea. Q J Eng Geol 22:31–48. https://doi.org/10.1144/gsl.qjeg.1989.022.01.03

Liu Z, Shao J, Xu W, Shi C (2013) Estimation of elasticity of porous rock based on mineral composition and microstructure. Adv Mater Sci Eng. https://doi.org/10.1155/2013/512727

Liu Z, Shao J, Xu W et al (2014) Prediction of elastic compressibility of rock material with soft computing techniques. Appl Soft Comput J 22:118–125. https://doi.org/10.1016/j.asoc.2014.05.009

Madhubabu N, Singh PK, Kainthola A et al (2016) Prediction of compressive strength and elastic modulus of carbonate rocks. Measurement 88:202–213. https://doi.org/10.1016/j.measurement.2016.03.050

Mahdiabadi N, Khanlari G (2019) Prediction of uniaxial compressive strength and modulus of elasticity in calcareous mudstones using neural networks, fuzzy systems, and regression analysis. Period Polytech Civ Eng 63:104–114. https://doi.org/10.3311/PPci.13035

Mallows CL, Sloane NJA (1973) An upper bound for self-dual codes. Inf Control 22:188–200. https://doi.org/10.1016/S0019-9958(73)90273-8

Manouchehrian A, Sharifzadeh M, Hamidzadeh Moghadam R, Nouri T (2013) Selection of regression models for predicting strength and deformability properties of rocks using GA. Int J Min Sci Technol 23:495–501. https://doi.org/10.1016/j.ijmst.2013.07.006

Marques EAG, Barroso EV, Filho APM, do Vargas EA (2010) Weathering zones on metamorphic rocks from Rio de Janeiro-Physical, mineralogical and geomechanical characterization. Eng Geol 111:1–18. https://doi.org/10.1016/j.enggeo.2009.11.001

Mashayekhi M, Kaliakin VN, Meehan CL et al (2020) Simulation of aggregate behavior in low confinement geotechnical applications. Comput Geotech 125:103678

Matin SS, Farahzadi L, Makaremi S et al (2018) Variable selection and prediction of uniaxial compressive strength and modulus of elasticity by random forest. Appl Soft Comput J 70:980–987. https://doi.org/10.1016/j.asoc.2017.06.030

Mielke PW Jr, Berry KJ (2001) Permutation methods: a distance function approach. Springer, New York (**ISBN 978-1-4757-3449-2**)

Mokhtari M, Behnia M (2019) Comparison of LLNF, ANN, and COA-ANN techniques in modeling the uniaxial compressive strength and static Young's modulus of limestone of the Dalan formation. Nat Resour Res 28:223–239. https://doi.org/10.1007/s11053-018-9383-6

Momeni A, Hashemi SS, Khanlari GR, Heidari M (2017) The effect of weathering on durability and deformability properties of granitoid rocks. Bull Eng Geol Environ 76:1037–1049. https://doi.org/10.1007/s10064-016-0999-7

Momeni E, Dowlatshahi MB, Omidinasab F, Maizir H, Armaghani DJ (2020) Gaussian process regression technique to estimate the pile bearing capacity. Arab J Sci Eng 45:8255–8267. https://doi.org/10.1007/s13369-020-04683-4

Nefeslioglu HA (2013) Evaluation of geo-mechanical properties of very weak and weak rock materials by using non-destructive techniques: ultrasonic pulse velocity measurements and reflectance spectroscopy. Eng Geol 160:8–20. https://doi.org/10.1016/j.enggeo.2013.03.023

Ocak I, Seker SE (2012) Estimation of elastic modulus of intact rocks by artificial neural network. Rock Mech Rock Eng 45:1047–1054. https://doi.org/10.1007/s00603-012-0236-z

Omoruyi F, Obubu M, Ifunanya O et al (2019) Comparison of some variable selection techniques in regression analysis. Am J Biomed Sci Res 6:281–293. https://doi.org/10.34297/AJBSR.2019.06.001044

Ozkat EC, Franciosa P, Ceglarek D (2017a) A framework for physics-driven in-process monitoring of penetration and interface width in laser overlap welding. Proc CIRP 60:44–49. https://doi.org/10.1016/j.procir.2017.01.043

Ozkat EC, Franciosa P, Ceglarek D (2017b) Laser dimpling process parameters selection and optimization using surrogate-driven process capability space. Opt Laser Technol 93:149–164. https://doi.org/10.1016/j.optlastec.2017.02.012

Ozkat EC, Franciosa P, Ceglarek D (2017c) Development of decoupled multi-physics simulation for laser lap welding considering part-to-part gap. J Laser Appl 29:022423. https://doi.org/10.2351/1.4983234

Pan J, Meng Z, Hou Q et al (2013) Coal strength and Young's modulus related to coal rank, compressional velocity and maceral composition. J Struct Geol 54:129–135. https://doi.org/10.1016/j.jsg.2013.07.008

Park YW, Klabjan D (2020) Subset selection for multiple linear regression via optimization. J Glob Optim 1:1–32. https://doi.org/10.1007/s10898-020-00876-1

Ranjbar-Karami R, Kadkhodaie-Ilkhchi A, Shiri M (2014) A modified fuzzy inference system for estimation of the static rock elastic properties: a case study from the Kangan and Dalan gas reservoirs, South Pars gas field, the Persian Gulf. J Nat Gas Sci Eng 21:962–976. https://doi.org/10.1016/j.jngse.2014.10.034

Rasmussen CE (2004) Gaussian processes in machine learning. Lect Notes Comput Sci. https://doi.org/10.1007/978-3-540-28650-9_4

Rezaei M (2018) Indirect measurement of the elastic modulus of intact rocks using the Mamdani fuzzy inference system. Measurement 129:319–331. https://doi.org/10.1016/j.measurement.2018.07.047

Rezaei M (2020) Feasibility of novel techniques to predict the elastic modulus of rocks based on the laboratory data. Int J Geotech Eng 14:25–34. https://doi.org/10.1080/19386362.2017.1397873

Rezaei M, Majdi A, Monjezi M (2014) An intelligent approach to predict unconfined compressive strength of rock surrounding access tunnels in longwall coal mining. Neural Comput Appl 24:233–241. https://doi.org/10.1007/s00521-012-1221-x

Roy GD, Singh TN (2018) Regression and soft computing models to estimate young's modulus of CO_2 saturated coals. Measurement 129:91–101. https://doi.org/10.1016/j.measurement.2018.07.016

Roy GD, Singh TN (2020) Predicting deformational properties of Indian coal: soft computing and regression analysis approach. Measurement 149:106975. https://doi.org/10.1016/j.measurement.2019.106975

Saedi B, Mohammadi SD, Shahbazi H (2018) Prediction of uniaxial compressive strength and elastic modulus of migmatites using various modeling techniques. Arab J Geosci 11:574. https://doi.org/10.1007/s12517-018-3912-9

Saedi B, Mohammadi SD, Shahbazi H (2019) Application of fuzzy inference system to predict uniaxial compressive strength and elastic modulus of migmatites. Environ Earth Sci 78:208. https://doi.org/10.1007/s12665-019-8219-y

Samui P, Kim D, Jagan J, Roy SS (2019) Determination of uplift capacity of suction caisson using gaussian process regression, minimax probability machine regression and extreme learning machine. Iran J Sci Technol Trans Civ Eng 43:651–657. https://doi.org/10.1007/s40996-018-0155-7

Shakoor A, Bonelli RE (1991) Relationship between petrographic characteristics, engineering index properties, and mechanical properties of selected sandstones. Environ Eng Geosci 28:55–71. https://doi.org/10.2113/gseegeosci.xxviii.1.55

Sharma VS, Sharma SK, Sharma AK (2008) Cutting tool wear estimation for turning. J Intell Manuf 19:99–108. https://doi.org/10.1007/s10845-007-0048-2

Singh TN, Verma AK (2012) Comparative analysis of intelligent algorithms to correlate strength and petrographic properties of some schistose rocks. Eng Comput 28:1–12. https://doi.org/10.1007/s00366-011-0210-5

Singh R, Kainthola A, Singh TN (2012) Estimation of elastic constant of rocks using an ANFIS approach. Appl Soft Comput J 12:40–45. https://doi.org/10.1016/j.asoc.2011.09.010

Singh R, Umrao RK, Ahmad M et al (2017) Prediction of geomechanical parameters using soft computing and multiple regression approach. Measurement 99:108–119. https://doi.org/10.1016/j.measurement.2016.12.023

Sonmez H, Tuncay E, Gokceoglu C (2004) Models to predict the uniaxial compressive strength and the modulus of elasticity for Ankara Agglomerate. Int J Rock Mech Min Sci 41:717–729. https://doi.org/10.1016/j.ijrmms.2004.01.011

Sonmez H, Gokceoglu C, Nefeslioglu HA, Kayabasi A (2006) Estimation of rock modulus: for intact rocks with an artificial neural network and for rock masses with a new empirical equation. Int J Rock Mech Min Sci 43:224–235. https://doi.org/10.1016/j.ijrmms.2005.06.007

Suykens JAK, Vandewalle J (1999) Least squares support vector machine classifiers. Neural Process Lett 9:293–300. https://doi.org/10.1023/A:1018628609742

Taylor KE (2001) Summarizing multiple aspects of model performance in a single diagram. J Geophys Res Atmos 106:7183–7192. https://doi.org/10.1029/2000JD900719

Tian H, Shu J, Han L (2019) The effect of ICA and PSO on ANN results in approximating elasticity modulus of rock material. Eng Comput 35:305–314. https://doi.org/10.1007/s00366-018-0600-z

Tiryaki B (2008) Predicting intact rock strength for mechanical excavation using multivariate statistics, artificial neural networks, and regression trees. Eng Geol 99:51–60. https://doi.org/10.1016/j.enggeo.2008.02.003

Torabi-Kaveh M, Naseri F, Saneie S, Sarshari B (2015) Application of artificial neural networks and multivariate statistics to predict UCS and E using physical properties of Asmari limestones. Arab J Geosci 8:2889–2897. https://doi.org/10.1007/s12517-014-1331-0

Tugrul A (2004) The effect of weathering on pore geometry and compressive strength of selected rock types from Turkey. Eng Geol 75:215–227. https://doi.org/10.1016/j.enggeo.2004.05.008

Umrao RK, Sharma LK, Singh R, Singh TN (2018) Determination of strength and modulus of elasticity of heterogenous sedimentary rocks: an ANFIS predictive technique. Measurement 126:194–201. https://doi.org/10.1016/j.measurement.2018.05.064

Undul O, Florian A (2015) Influence of micro-texture on the geo-engineering properties of low porosity volcanic rocks. Eng Geol Soc Territ 6:69–72. https://doi.org/10.1007/978-3-319-09060-3_12

Vapnik VN (1995) The nature of statistical learning theory. Springer, New York, p 187 (**ISBN 0-387-94559-8**)

Wang HY, Ding WX, Yang JJ (2014) Study on the engineering properties of saturated red sandstone. Appl Mech Mater 638:589–593

Willmott C, Matsuura K (2005) Advantages of the mean absolute error (MAE) over the root mean square error (RMSE) in assessing average model performance. Clim Res 30:79–82

Willmott CJ, Matsuura K, Robeson SM (2009) Ambiguities inherent in sums of squares based error statistics. Atmos Environ 43:749–752. https://doi.org/10.1016/j.atmosenv.2008.10.005

Wyering LD, Villeneuve MC, Wallis IC et al (2014) Mechanical and physical properties of hydrothermally altered rocks, Taupo Volcanic Zone, New Zealand. J Volcanol Geotherm Res 288:76–93. https://doi.org/10.1016/j.jvolgeores.2014.10.008

Xia M, Zhao C, Hobbs BE (2014) Particle simulation of thermally-induced rock damage with consideration of temperature-dependent elastic modulus and strength. Comput Geotech 55:461–473. https://doi.org/10.1016/j.compgeo.2013.09.004

Yagiz S, Sezer EA, Gokceoglu C (2012) Artificial neural networks and nonlinear regression techniques to assess the influence of slake durability cycles on the prediction of uniaxial compressive strength and modulus of elasticity for carbonate rocks. Int J Numer Anal Methods Geomech 36:1636–1650. https://doi.org/10.1002/nag.1066

Yasar E, Erdogan Y (2004) Correlating sound velocity with the density, compressive strength and Young's modulus of carbonate rocks. Int J Rock Mech Min Sci 41:871–875. https://doi.org/10.1016/j.ijrmms.2004.01.012

Yilmaz I (2009) A new testing method for indirect determination of the unconfined compressive strength of rocks. Int J Rock Mech Min Sci 46:1349–1357. https://doi.org/10.1016/j.ijrmms.2009.04.009

Yilmaz I, Yuksek AG (2008) An example of artificial neural network (ANN) application for indirect estimation of rock parameters. Rock Mech Rock Eng 41:781–795. https://doi.org/10.1007/s00603-007-0138-7

Yilmaz I, Yuksek G (2009) Prediction of the strength and elasticity modulus of gypsum using multiple regression, ANN, and ANFIS models. Int J Rock Mech Min Sci 46:803–810. https://doi.org/10.1016/j.ijrmms.2008.09.002

Zhang L (2017) Evaluation of rock mass deformability using empirical methods—a review. Undergr Space 2:1–15. https://doi.org/10.1016/j.undsp.2017.03.003